2011
2012

GENEESKUNDE

master in de biomedische wetenschappen: bio-elektronica en nanotechnologie

Masterproef

Characterization of carbon nanosheets as an electrode material and biological interface for advanced microelectrode arrays

Promotor :
Prof. dr. Patrick WAGNER

Promotor :
dr. DRIES BRAEKEN

Jordi Cools

Masterproef voorgedragen tot het bekomen van de graad van master in de biomedische wetenschappen , afstudeerrichting bio-elektronica en nanotechnologie

De transnationale Universiteit Limburg is een uniek samenwerkingsverband van twee universiteiten in twee landen: de Universiteit Hasselt en Maastricht University

universiteit hasselt
KNOWLEDGE IN ACTION

Maastricht University

Universiteit Hasselt | Campus Diepenbeek | Agoralaan Gebouw D | BE-3590 Diepenbeek
Universiteit Hasselt | Campus Hasselt | Martelarenlaan 42 | BE-3500 Hasselt

Maastricht University

universiteit hasselt
KNOWLEDGE IN ACTION

2011
2012

GENEESKUNDE

master in de biomedische wetenschappen: bio-elektronica en nanotechnologie

Masterproef

Characterization of carbon nanosheets as an electrode material and biological interface for advanced microelectrode arrays

Promotor :
Prof. dr. Patrick WAGNER

Promotor :
dr. DRIES BRAEKEN

Jordi Cools

Masterproef voorgedragen tot het bekomen van de graad van master in de biomedische wetenschappen , afstudeerrichting bio-elektronica en nanotechnologie

Maastricht University

universiteit hasselt
KNOWLEDGE IN ACTION

ά{Ι·ΰΛăƬΙ·ŎΰΛ2ƴ2Ƭ 2yŜ℁ă ŎdzℕΛ2ăΛΰë ΛĂ 2yŜ 2Ƭ ΰKŜ ∃ℕŜΙ·ΰŜăΰ ă2dzℕŎŜă 2Ƭ KΙ·LJLJΛyŜăă ΛƴſΛŦŜ."

Dr. Linus Pauling

Contents

Abbreviations

AP	Action potential
aSi	Amorphous silicon
Calcein AM	Acetomethoxy derivate of calcein
CMOS	Complementary metal-oxide-semiconductor
CNS	Carbon nanosheet
CNT	Carbon nanotube
CPE	Constant phase element
$CSC_{(C)}$	(Cathodal) charge storage capacity
CV	Cyclic voltammetry
CVD	Chemical vapor deposition
DOS	Density of states
EIS	Electrochemical impedance spectroscopy
ET	Electron transfer
IC	Integrated circuit
MEA	Micro- (or multi-)electrode array
MPECVD	Microwave plasma-enhanced chemical vapor deposition
OCP	Open-circuit potential
PBS	Phosphate buffered saline
PDMS	Polydimethylsiloxane
PECVD	Plasma-enhanced chemical vapor deposition
PI	Propidium Iodide
PLL	Poly-L-lysine
R_{CT}	Charge-transfer resistance
R_S	Solution resistance
TiN	Titanium nitride
TiO_2	Titanium dioxide
UV/O_3	UV/ozone
XSEM	Cross-sectional scanning electron microscopy
Z_{CPA}	Constant phase angle impedance
Z_W	Warburg impedance

Preface

Before I start off by thanking everyone who made this thesis possible, I would first like to extend a word of gratitude to a person whom I have not met for at least five years now. 'Coach' Johnny Jordens, my former science teacher in high school, thank you for everything you have taught me. If it were not for you, I probably would not have been writing this thesis as a future Master in Bioelectronics and Nanotechnology. Ever since we paid a visit to imec, I was absolutely convinced to continue my education in the field of science, and determined to someday work for this company. I sincerely hope we meet again soon.

I would like to give special thanks to my promotor at imec, Dr. Dries Braeken, who gave me the opportunity to work in his group and to let me experience what it is like to conduct fundamental and leading-edge scientific research. I admire your knowledge, experience and work as the *in vitro* team leader, and you have become a role model for my future career. Also Danielle Rand, thank you for your input and time to read this thesis thoroughly. You made me appreciate electrochemistry far more than I ever had, and you introduced me to a good friend which I never thought it would be, the Autolab. I am also grateful to Nadine Collaert, who helped me out during the first few months of my internship and assisted me whenever possible. I wish you all the success and happiness in your new position. I would also like to thank Karen van Keer and Olga Krylychkina for performing the cell cultures, and for all the funny moments we shared. Next, a big appreciation to the rest of my dear colleagues; Danny, Liesbeth, Silke, Dimiter, Luis, Katrien, Andim, Sébastien, Carmen, Alex, Carolina, Wolfgang and everybody else of the BIONE group, whose friendship I deeply treasure. I would also like to give special thanks to my internal promotor and coordinator of the Bioelectronics and Nanotechnology Master programme, Prof. Dr. Patrick Wagner, and my second examiner Prof. Dr. Miloš Nesládek. Last, but not least, I would like to thank my mother for her moral support, and to give me the opportunity to undertake these studies, and Yanick, my girlfriend, who I love with all my heart and soul.

Abstract

In order to advance our knowledge about intercellular communication, high-throughput systems that are able to perform single-cell measurements are of great interest. Microelectrode arrays (MEAs) integrate micron-sized electrodes on a planar substrate to realize electrophysiological measurements with high spatial and temporal resolution. The acquisition of adequate electrogenic cell signals, however, depends highly on the interface between the biological and electronic system. Biocompatibility, inertness, low impedance and good capacitive coupling, together with good mechanical and electrical stability, are all prerequisites when seeking novel electrode materials.

Carbon nanosheets (CNSs) are an emerging type of carbon (nano)material, with many fascinating properties that have yet to be explored. Carbon nanosheets consist of multiple layers of graphene which are structured in such a way that they are oriented vertically on the substrate. Their high surface-area-to-volume ratio and abundance of active knife-edge planes make CNSs an attractive candidate for a new electrode material for bidirectional interfacing with electrogenic cells. Because CNSs are inherently hydrophobic, methods to improve wettability, and thus biocompatibility, were investigated, including voltage-biasing and a UV/ozone treatment. The CNSs were then electrochemically characterized using cyclic voltammetry and electrochemical impedance spectroscopy in order to assess the material's stimulation and recording capabilities, respectively. Our results demonstrate that a 90% reduction in electrode impedance and a 330% increase in cathodal charge storage capacity is achievable using these surface treatments. Furthermore, biocompatibility was assessed by culturing primary mouse hippocampal neurons on CNS substrates, which, to our knowledge, has not been demonstrated to date. We found that cell viability on surface-treated CNS electrodes subsequently coated with poly-L-lysine was vastly improved from non-treated CNSs. Our findings demonstrate that CNS-based MEAs can have a major scientific and technological impact, and combined with complementary metal-oxide-semiconductor integrated circuit technology, can yield tools for both *in vitro* and *in vivo* applications, including pharmacology, medical diagnostics, neuroscience and neuromedical research.

Abstract

Om onze kennis over intercellulaire communicatie te verruimen is het van groot belang om systemen te ontwikkelen die individuele celmetingen kunnen uitvoeren met een hoge verwerkingscapaciteit. Microelectrode arrays (MEAs) integreren microelektroden op een vlak substraat om elektrofysiologische metingen te realiseren met een hoge ruimtelijke en temporele resolutie. Het verwerven van adequate signalen van elektrogene cellen is echter sterk afhankelijk van het grensvlak tussen het biologische en elektronische systeem. Biocompabiliteit, chemische inertie, een lage impedantie en een goede capacitieve koppeling, samen met een goede mechanische en elektrische stabiliteit, zijn allemaal belangrijke eigenschappen bij het zoeken naar nieuwe elektrodematerialen.

Carbon nanosheets (CNSs) zijn een nieuw type koolstof (nano)materiaal, met vele fascinerende eigenschappen die nog nader onderzocht moeten worden. CNSs bestaan uit meerdere lagen grafeen die zo gestructureerd zijn dat ze verticaal georienteerd zijn op het substraat. Hun hoge oppervlakte-volume verhouding en overmaat aan scherpe vlakken maken van CNSs een veelbelovende kandidaat als nieuw elektrodemateriaal voor de bidirectionele interfacing met elektrogene cellen. Wegens hun inherente hydrofobiciteit werden methoden onderzocht om de bevochtigbaarheid van CNSs, en dus hun biocompatibiliteit, te laten toenemen. Zo kunnen CNSs elektrochemisch geoxideerd worden door middel van een voltage, of behandeld worden met UV/ozon. De CNSs werden vervolgens elektrochemisch gekarakteriseerd met behulp van cyclische voltammetrie en elektrochemische impedantiespectroscopie om hun respectievelijke stimulatie- en opnamecapaciteit te evalueren. Onze resultaten tonen aan dat deze oppervlaktebehandelingen de impedantie van de elektrode met 90% kunnen verminderen, en de kathodische ladingsopslagcapaciteit met 330% kunnen laten toenemen. Bovendien werd de biocompatibiliteit geëvalueerd door primaire hippocampale neuronen van muizen te groeien op CNS substraten, iets wat, voor zover wij weten, tot op heden nog niet is aangetoond. We stelden vast dat de levensvatbaarheid van cellen op oppervlaktebehandelde CNS elektroden, gecoat met poly-L-lysine, sterk toenam vergeleken met onbehandelde CNSs. Onze bevindingen tonen aan dat CNS-gebaseerde MEAs een belangrijke wetenschappelijke en technologische impact kunnen hebben, en gecombineerd met complementaire metaal-oxide-halfgeleider chiptechnologie een belangrijke bijdrage kunnen leveren voor (zowel *in vitro* als *in vivo*) toepassingen in de farmacologie, medische diagnostiek, neurowetenschap en neuromedisch onderzoek.

1. Introduction

Ever since the discovery that the brain is the center of our thoughts, movements and emotions, it has been an arduous task to unravel its complex biology and physiology. While much is known about the brain's structure and functioning *an sich*, one question that still plagues researchers for decades is how this consistent communication between an enormous amount of neurons is orchestrated. Although this research is still in its early stages, important new methods and techniques to study neuron (or any other electrogenic cell in general) dynamics are rapidly emerging. However, for a deep, comprehensive understanding of these mechanisms it is highly desirable to address single cells.[1-3] One widespread technique and a *de facto* standard to study electrophysiological phenomena in single cells is the patch clamp technique, which makes use of a glass micropipette that makes contact with ion channels in the cell membrane to measure transmembrane currents.[4-6] Although this technique has proven its usefulness, it also suffers from significant drawbacks, such as its technical difficulty, limited output and large costs.[7] Moreover, patch clamping is an invasive method as the tip of the micropipette damages the cell membrane; in able to gain electrical access to the cell, the membrane inside the pipette is ruptured. Moreover, there is significant washout or diffusion from pipette to cell and vice versa.[6] For these reasons, new (*in vitro* and *in vivo*) cellular interfacing technologies are currently being developed. One promising and fast-growing technology is the microelectrode array (MEA). As the name suggests, MEAs are arrangements of micron-sized electrodes that allow for the observation of spatiotemporal patterns of electrogenic cell activity. Using standard photolithographic techniques, MEAs can currently be fabricated with electrode dimensions smaller than the size of a typical mammalian cell (10 µm).[1, 2, 8, 9] This allows for stimulation and recording on the single-cell level with high resolution.

In order to achieve a high signal-to-noise ratio it is necessary to have intimate cell-electrode contact.[10, 11] Spatial proximity affects both the recording as stimulation efficiency of the electrode; a relatively large distance between electrode and cell decreases the ability to record low voltages (i.e. small signals), while at the same time the voltage or current needed to deliver the same amount of charge for stimulation would be higher.[12] Thus, in order to achieve a good cell-electrode contact, the physicochemical environment of the cells should be designed to foster and promote both cell growth and survival. This implies that the electrodes must be stable, inert, corrosion-free and biocompatible. Furthermore, adequate (capacitive) signal sensing of the electrodes requires a low impedance, while at the same time a high charge storage capacity (CSC) is necessary for stimulation (see section 1.2).**[13]** These properties are mainly dependent on the electrochemical characteristics of the electrode material, and several different materials have already been implemented as MEA electrodes. Some examples include TiO_2[8], TiN[1, 14, 15], Pt-black[16-18], indium tin oxide[19], Au[20] and carbon nanotubes (CNTs)[21-24]. The biocompatibility and cellular adhesion can be further increased by (bio)functionalizing the electrodes with charged chemical groups or specific biomolecules, which will be explained in the following sections.

In the present study, we investigate the role of carbon nanosheets (CNSs) as the interface between biological and electronic systems. The highly graphitized, flake-like structure of CNSs yields a high surface-area-to-volume ratio and renders numerous interaction points for the cells to adhere to. This, together with the

abundance of active knife-edge planes, makes CNSs a promising interface material for high-quality MEA measurements. Using cyclic voltammetry (CV) and electrochemical impedance spectroscopy (EIS), the CNSs were electrochemically characterized and further modified for optimal recording and stimulation. Furthermore, biocompatibility was assessed by culturing mouse hippocampal neurons on CNS substrates, which, to our knowledge, has not been demonstrated to date.

The applications and advantages of MEAs over conventional electrophysiological methods (e.g. patch clamping and single electrode recording) are numerous. Large amounts of individually addressable electrodes are able to gain information from multiple cells at a time, at different locations in the same tissue and over a long period of time. This makes MEAs ideal *in vitro* systems to study both acute and chronic (pharmacological) effects of drugs and toxins, and the biophysical aspects of network formation, activity and remodeling.[25]

1.1 Neuron Dynamics

The stimulation and recording of electrogenic cells requires a comprehensive understanding of the basic bioelectrical phenomena underlying cell-to-cell communication. Electrically excitable cells such as neurons, cardiomyocytes (heart cells) and muscle cells use action potentials (APs) to communicate with each other. As neurons are the main excitable cells of the body with the simplest conduction mechanism, we will only explain neuronal AP initiation and propagation.

The three main parts of a neuron are called the soma (cell body), dendritic tree and axon (**Fig. 1**). The highly branched dendrites form the input side of the neuron and receive electrical signals from axons of other neuronal cells. The axon can be regarded as the output side and conducts or transmits the AP to other neurons. In their resting state, neurons have a potential difference across their membrane of approximately -70 mV.[26] This potential is maintained by membrane-bound proteins that can either actively or passively transport ions (i.e. Na^+, Cl^-, K^+,...) into or out of the cell[27-29]. When the input signals reach the soma through the dendrites, they are spatiotemporal summated and can either cause excitation or inhibition; that is, increase (depolarize)

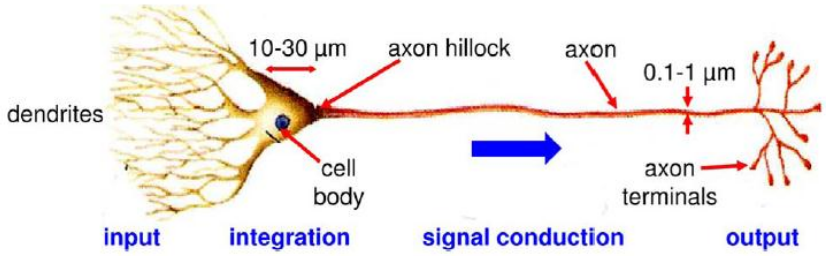

Fig. 1. Morphology of a typical neuron. The cell body or soma receives input from the dendrites and can propagate the signal further to other neurons through the axon, which in its turn makes contact to other cells (figure adopted from [30]).

or decrease (hyperpolarize) the membrane potential of the neuron.[31] Only when a depolarizing signal causes the membrane potential to reach a certain threshold value, the neuron will produce an AP that propagates through its axon to other neurons.[32] The change of the membrane potential is mediated by the opening or closing of voltage-gated ion channels, i.e. the flow of ions into or out of the cell (**Fig. 2**).[29, 33] When the membrane potential reaches the threshold potential (≈ -55 mV), the Na^+ channels open and a large influx of Na^+ ions causes a rapid depolarization of the membrane potential.[32] Right before the Na^+ channels close, the K^+ channels open and K^+ starts to leave the cell. Once the Na^+ channels are completely closed the efflux of K^+ causes the membrane potential to become more negative again. Once it reaches its normal resting potential of approximately -70 mV, the K^+ channels close and the Na^+/K^+ pump starts to actively transport Na^+ out of the cell and K^+ into the cell, so that the next AP can occur.[28] This sequence of events takes 2-3 ms to complete.[30]

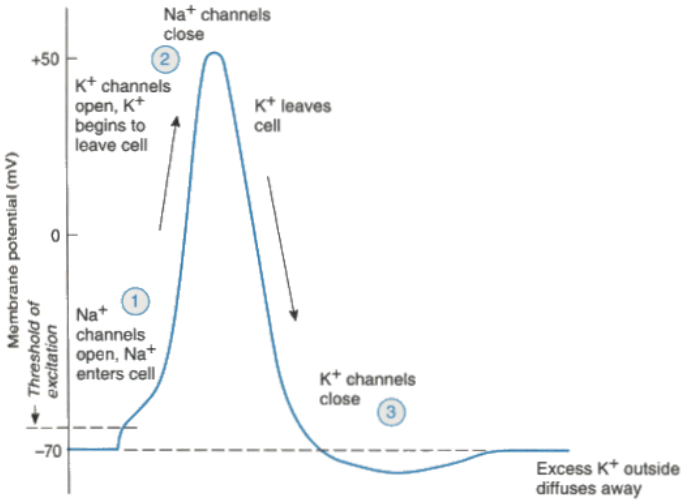

Fig. 2. Form of a neuronal action potential (AP), generated by the cooperation between voltage-dependent Na^+ and K^+ channels (figure adopted from [34]).

1.2 Microelectrode Arrays (MEAs) and the Electrode/Electrolyte Interface

As briefly described previously, MEAs make use of an ordered array of non-invasive extracellular electrodes to achieve high spatial and temporal resolution. Several MEA systems are currently commercially available, one of the principal manufacturers being Multi Channel Systems (MCS) GmbH (Germany). However, the amount of electrodes on these MEA systems is still rather limited (typically an array has approximately 60 electrodes with a 10 µm diameter).[30] Commercially available MEAs are thus not suited for high-throughput experiments. As this is a highly wanted feature for, for example, large scale, *in vitro* pharmaceutical drug screening applications, it is necessary to both increase the number of electrodes and make them smaller, so that single-cell addressability can be achieved. This has already been demonstrated by several authors, who presented an *in vitro* MEA with 16,384 individually addressable, subcellular-sized (diameters ranging from 1.2-

4.5 µm) electrodes. [1, 2, 8, 9] An example of such a MEA, fabricated by imec, is shown in **Fig. 3**. Another drawback of commercially available MEAs are that they are *passive* systems, meaning that each electrode needs a connection to external circuitry, which is one of the reasons that their number of electrodes is limited.[30] The use of custom-fabricated, passive components also makes them expensive, reduces their lifetime and, most importantly, prevents them from processing the recorded signals autonomously.[35]

As a consequence, microarrays are being integrated with complementary metal-oxide-semiconductor (CMOS) integrated circuit (IC) technology. In these *active* microarrays, the circuitry components form an integral part of the transducer system, as they are integrated with the electrodes on the same substrate.[30] Using this technology, the number of electrodes can be increased drastically.[1, 8, 9] Furthermore, it gives advantages with respect to connectivity, signal quality and (less significantly) ease of handling and use.[30] CMOS IC technology is also a standardized technique that will eventually allow for the large-scale production of low-cost MEAs.[35]

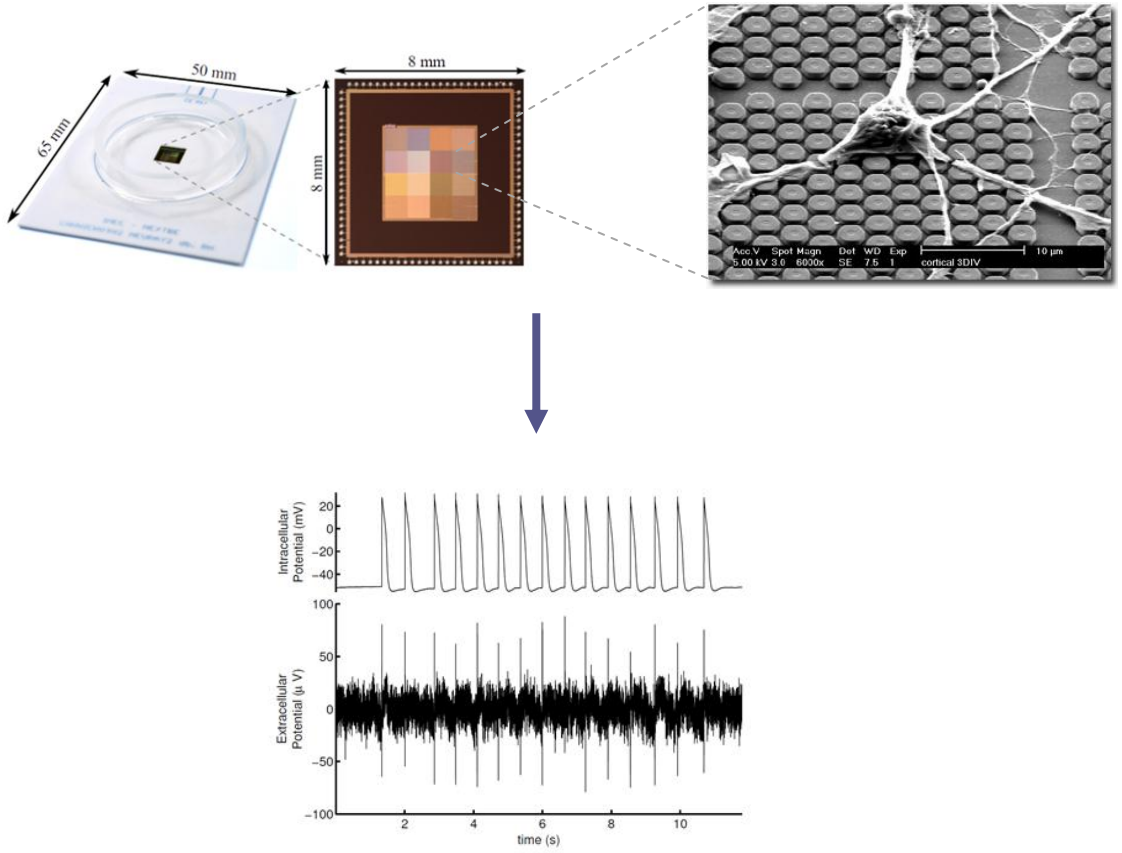

Fig. 3. Single-cell microelectrode array (MEA) for the recording of electrical signals from electrogenic cells (MEA fabricated by imec).

As explained in the previous section, APs are the result of the subsequent depolarization and repolarization of the cellular membrane through the in- and efflux of ions. It is these local variations of the electrical potential that can be extracellularly measured by the MEAs. Ideally, the signals are recorded with a high signal-to-noise ratio and a high spatiotemporal resolution. There is, however, an important restriction that

must be taken into consideration. A high spatial and temporal resolution implies that the size of the electrodes must be as small as possible, but scaling down their dimensions also yields a corresponding increase in impedance, and thus more noise.[11] This relationship can be expressed as:

$$V_{el,noise} = \sqrt{4kTR_N\Delta f} \quad [1]$$

where $V_{el,noise}$ is the electrode noise voltage, kT is the product of the Boltzmann constant and the temperature, R_N is the equivalent noise resistance (i.e. the real part of the electrode impedance magnitude) and Δf is the recording bandwidth. It is therefore of high importance to choose a proper electrode material which yields a low impedance for MEA measurements.

Regarding the assessment of the impedance and other characteristics of the electrode/electrolyte interface, several equivalent circuit models have been developed that aid researchers to understand the electrical phenomena that occur when an electrode stimulates or records a cell.[30, 36, 37] **Fig. 4(a)** shows the most commonly used equivalent circuit model of the electrode/electrolyte interface. The different elements that make up the model are a constant-phase-angle impedance Z_{CPA}, a charge-transfer resistance R_{CT}, the Warburg impedance Z_W and a solution resistance R_S. Generally, Z_{CPA} describes the behavior of a double layer or imperfect capacitor and is given by:

$$Z_{CPA} = \frac{1}{Q_0(i\omega)^n} \quad [2]$$

where Q_0 is a constant with dimensions $S.s^n$ *, $i = \sqrt{-1}$, ω is the angular frequency and $-1 < n < 1$ (related to surface irregularities).[38] When $n = 1$ the equation describes a perfect capacitor, but in reality n is always less than 1. The Warburg impedance Z_W takes into account that chemical reactants or ions in solution (produced on the surface of the electrode) need to diffuse away.[30] For high frequencies (above 1 Hz), the Warburg impedance becomes negligible and does not significantly contribute to the overall impedance.[39] The frequency range that is most concerned with in this work is 1 kHz, as this is the characteristic frequency in the power spectrum of a neural AP (with a duration of 1 ms), and thus the frequency by which electrodes are usually characterized.[32] The resistance between the electrode under investigation and counter electrode, or solution resistance R_S, can also principally be neglected as its magnitude is only several kΩ.[30] Overall, Fig. 4(a) can be transformed to a simplified model which is presented in **Fig. 4(b)**. It includes the charge-transfer resistance R_{CT} in parallel with a capacitor C_E, the latter of which corresponds to the thin electrical double layer at the electrode/electrolyte interface that arises by the fast charge separation when a voltage is applied.[40]

Regarding the constant-phase-angle impedance Z_{CPA}, its value is actually the impedance of the so-called constant phase element (CPE). Although the physical meaning of this element is not clear, it is a frequently used component when experimental impedance data are fitted in equivalent electrical circuits. As briefly mentioned above, it describes a perfect capacitor for $n = 1$, a resistor for $n = 0$, and an inductor for $n = -1$.[38, 41, 42] This complex behavior is generally attributed to a number of phenomena, including surface

* S = siemens; the SI unit of electrical conductance; the reciprocal of one ohm.
s = the SI unit of second.

roughness and reactivity, varying thickness or composition of the coating, the porosity of the electrode and non-uniform current distribution (i.e. 'edge effects').[38]

The characterization of electrodes also often involves the determination of their cathodal charge storage capacity (CSC_c), which is a measure of the total charged stored within the electrode available for a stimulation pulse (the CSC_c is the time integral of negative current in the cyclic voltammogram).[13] For more information about electrode characterization we refer to [13].

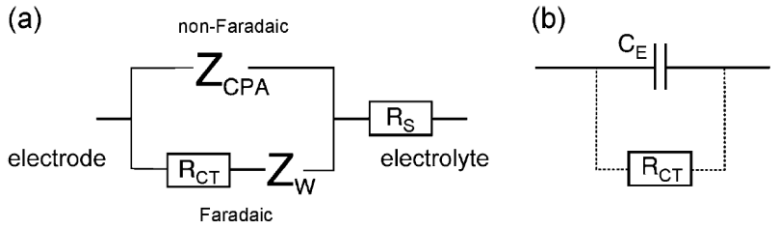

Fig. 4. (a) Equivalent circuit of the electrode/electrolyte interface. The constant-phase-angle impedance Z_{CPE} lies in parallel with the charge-transfer resistance R_{CT} and the Warburg impedance Z_W. R_S is the resistance of the solution. (b) Simplified model of (a), where Z_{CPA} is replaced by a capacitor C_E, parallel to R_{CT} (figure adopted from [30]).

1.3 Carbon Nanosheets

Carbon nanosheets (CNSs; sometimes also referred to as carbon nanowalls, nanoflakes or petals) consist of multiple layers of graphene which are structured in such a way that they are oriented vertically on the substrate (**Fig. 5**). The initial method of synthesis of graphene involved elaborate techniques such as the micromechanical cleaving of bulk graphite[43], chemical exfoliation[44], epitaxial growth[45] and thermal decomposition of silicon carbide (SiC).[46, 47] Nowadays, the standard process is microwave plasma-enhanced chemical vapor deposition (MPECVD), which enables the (catalyst-free) growth of CNSs with a growth rate of about 1.5 µm min^{-1} at temperatures as low as 500°C.[48-51] Recently, Zhang et al. even reported a new technique to grow CNSs at temperatures below 100°C, based on ultrasonic spray pyrolysis.[52] As shown in **Fig. 5**, the CNSs consist of a relatively broad base which constantly narrows along the growth direction. The flake edges have a highly graphitized knife-edge structure and are only 1-3 graphene layers (2-3 nm) thick. The spacing between the planes is in the range between 0.345-0.36 nm.[49]

Two properties of CNSs make them very interesting for potential electrode material applications. First, their flake-like structure results in a high surface-area-to-volume ratio, ensuring numerous interaction points for cells to adhere to. Second, and most importantly, in contrast to the nearly inert basal planes, the edge planes contain many open graphitic layers and steps (crystal defects) which are highly reactive.[49] Due to the difference in the density of states (DOS) near the Fermi level, these defects show remarkable electron transfer (ET) kinetics, and active electrocatalytic and biosensing properties.[49, 50] Moreover, the edges can easily be (bio)functionalized and can serve as potential adsorption sites for e.g. hydrogen and oxygen species.[49]

Concerning the use of carbon nanomaterials as electrodes for extracellular neuronal recording, carbon nanotubes (CNTs) have also attracted significant interest in the last several years.[21, 53-55] Carbon nanotubes

have proven to be an effective electrode material with high electrical conductivity, intrinsically large surface areas and good biocompatibility.[56] However, the synthesis of CNTs still relies on the use of metal catalysts (e.g. Fe, Ni, Co or Mo).[57] The presence of these residual metal particles can lead to potential misinterpretations of electrochemical experiments and can significantly affect their electrochemical repeatability and stability.[58] Moreover, the bioavailability of these catalysts might also contribute to harm the cells.[59] The capillary action of water can also cause accumulation of the CNTs, which can be favorable for the fabrication of complex surface architectures[60-62], but not for the purpose considered here. Unlike CNTs, CNSs are grown completely catalyst-free and do not accumulate together, two properties that contribute to their high electrochemical stability.

As the number of published articles about CNSs is relatively scarce to date, our experimental approach will be partly built on research performed on CNTs. One example of a biomedical application that has already been accomplished is the biological modification of CNSs with DNA strands[63], but to date the interaction of CNSs with cells is still unknown. In order to make CNSs more hydrophilic and thus biocompatible, they can be exposed to a UV/ozone (UV/O_3) treatment, which in the case of CNTs yields a lower interfacial impedance, higher capacitance and higher neuron-cell densities.[21] The same results were found with CNTs that were functionalized with positively charged molecules.[22, 64] Cellular adhesion can also be increased by coating the surface with poly-L-lysine (PLL)[65] or exploiting the binding capabilities of integrins, proteins which are naturally present on the cell surface.[20, 29] For example, integrins are known to show a strong binding affinity with laminin.[66, 67] By applying an oxygen plasma treatment to their CNT/chitosan fiber surface, followed by a subsequent coupling of laminin, Huang et al. increased the cell adhesion ratio from 3.2% to 72.2%.[68] In the present study, biocompatibility is assessed by the culture of primary (mouse) hippocampal neurons on both pristine and surface-treated CNS substrates. Cell viability is evaluated by differentially labeling live and dead cells and fluorescence microscopy.

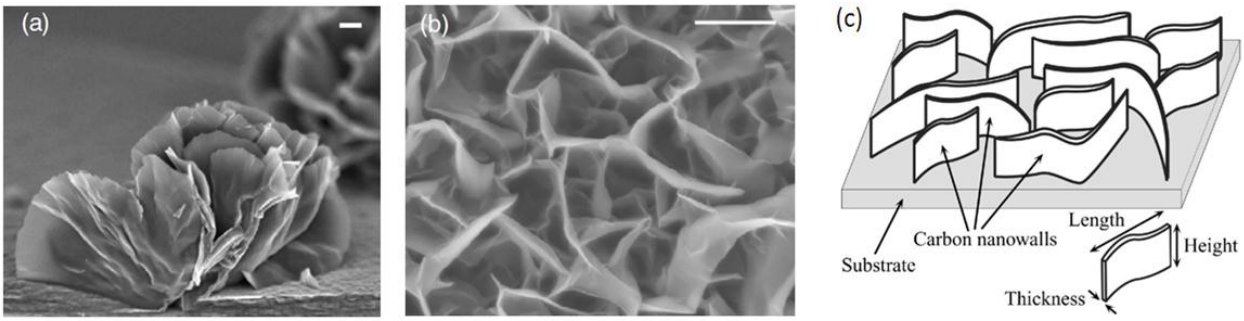

Fig. 5. (a) SEM image of freestanding CNSs, displaying the typical dimensions and orientation. (b) Top view SEM image showing high density flakes. Both scale bars correspond to 1 µm (figures adopted from [48]). (c) Schematic illustration of the vertically aligned graphitic sheets. The general morphology of carbon nanowalls is virtually identical to CNSs (figure adopted from [69]).

1.4 Research Question

The acquisition of adequate electrogenic cell signals (using *in vitro* interface platforms) depends highly on the interface used between the biological and electronic system. Biocompatibility, inertness, low impedance and good capacitive coupling, together with good mechanical and electrical stability, are all highly wanted features for novel electrode materials. The disadvantage of current commercially available MEA platforms is that they suffer from a low simultaneous output of signals and are therefore not used for high-throughput experiments.[30] Moreover, these systems make use of passive, custom-fabricated components which makes them expensive and prevents them from processing the recorded signals autonomously.[35] It is therefore important to scale down the size of the electrodes without a consequent increase in impedance. Because of these reasons, carbon nanomaterials are currently on the forefront as new electrode materials. Although CNTs have recently been implemented as neuro-electronic interconnects, water can cause the CNTs to accumulate, and their residual metal nanoparticles can cause harm to the cells and misinterpretations of electrochemical experiments.[58]

Given the background information described above, CNSs are an attractive candidate for a new electrode material for bidirectional interfacing with electrogenic cells in a MEA setting. The combination of a high surface-area-to-volume ratio and abundance of highly reactive edge planes is expected to give rise to a good electrical coupling for recording and stimulation. To test whether CNSs can be implemented in a high-throughput MEA setup, electrochemical characterization using CV profiling and EIS will be performed. Together with some wet chemistry based preliminary treatments, we will examine how the impedance can be reduced as low as possible and how the highest CSC_c can be obtained, i.e. if CNSs are suited for stimulation and recording experiments on electrogenic cells. Next, primary mouse hippocampal neurons will be cultured on the CNSs to test biocompatibility, cell adhesion, specific growth and interaction with the material. The outcome of these results will eventually determine if the step to patterned, micron-sized electrodes is warranted for further MEA experiments. Combined with CMOS IC technology, this new electrode material can lead to more sensitive and cheaper MEAs, which is beneficial for pharmaceutical drug screening applications (e.g. investigating dose-related effects of drugs), and both *in vitro* as *in vivo* applications in neuroscience and neuromedical research.

2. Materials & Methods

2.1 Preparation and Characterization of CNSs

Substrates consisted of 300 nm thermal SiO_2 grown on a 200 nm Si (p-type) wafer. A 300 nm TiN layer was sputtered from a Ti target in a N_2 atmosphere (Applied Endura Extensa TTN). Carbon layers were grown in a low pressure (0.5 Torr) 13.56 MHz RF generator (Oxford Instruments plasma technology UK NANOCVD). In a typical CNS growth experiment a 200 mm wafer was allowed to reach a heater temperature of 750°C under vacuum (1 x 10^{-5} Torr) for 1 min. To prepare the wafer surface, a H_2 plasma pretreatment (300 W) was carried out for 15 min at 0.5 Torr. Methane (CH_4; 50 sccm) or acetylene (C_2H_2; 10 sccm) were flowed into the chamber in a CH_4/H_2 ratio of 1:2 or 1:10 for C_2H_2/H_2 and a 300 W plasma at a total pressure of 0.5 Torr was maintained. The substrate was removed from the chamber and allowed to cool under vacuum (1 x 10^{-4} Torr) for 5 min.

Initially, CNSs were grown on two different substrates, i.e. amorphous silicon (aSi) and titanium nitride (TiN). For the electrochemical characterization, the wafer substrates were cleaved to a size of approximately 2 x 4 cm, upon which an active electrode area of about 2 cm^2 (Ø 1.6 cm) was delimited with polydimethylsiloxane (PDMS). The samples were subsequently cured in an oven at 110°C for 15 min.

Carbon nanosheet samples were electrochemically characterized using an Autolab PGSTAT302N potentiostat/galvanostat instrument from Metrohm, controlled by the NOVA software (version 1.8, Ecochemie, Netherlands). The setup consisted of a three-electrode system in a glass beaker placed inside a Faraday cage; a commercial double-junction Ag|AgCl (3 M KCl) reference electrode (Radiometer Analytical, France), a large-area Pt counter electrode coil, and a working electrode that was attached to the CNS sample. The electrolyte consisted of a phosphate buffered saline (PBS; 0.150 M NaCl, 0.016 M Na_2HPO_4, 0.004 M KH_2PO_4, pH 7.4) solution at 25°C. All chemicals were analytical grade and used as delivered (Sigma-Aldrich, USA). Cyclic voltammetry and EIS measurements were performed with respect to the open-circuit potential (OCP). The sweep rate of the CV measurements was fixed at 0.5 V/s, with linear scans between a lower vertex potential of -1.0 V and an upper vertex potential of 1.1 V. The number of potential crossings was set to 20 (i.e. 10 cycles), with the 10^{th} cycle values each time extracted for comparative results. For EIS measurements, a frequency response analysis (FRA) frequency scan was performed between 100 kHz and 0.01 Hz with an AC amplitude of 0.01 V(ms).

Cross-sectional scanning electron microscopy (XSEM) was performed using a XL-30 (Philips) SEM. To evaluate the degree of wettability, static sessile contact angle measurements were made with distilled water at ambient temperature using an OCA 20 goniometer (Dataphysics, Germany). The water droplets had a volume of 1 µl and were dispensed using a computer-controlled automatic liquid dispensing system. For each experiment the average static contact angle for water was measured.

2.2 CNS Sample Treatments

Different sample treatments on CNSs were performed to study the effect on CSC_c, impedance, hydrophilicity and biocompatibility. UV/O_3 treatments were performed using an UVO Cleaner 144AX from Jelight Company Inc. For the voltage-bias experiments, 10 s biphasic voltage pulses ranging from 1 to 2 V were applied to the samples, which were electrochemically characterized after each set of 10 pulses. By integrating and summing the resulting anodal currents (the cathodal currents can also be used), the charge density delivered at the anodic phase was calculated (in C cm^{-2} ph^{-1}; **Fig. 6**). Voltage-biasing was performed with the previously described setting, i.e. the Autolab PGSTAT302N potentiostat/galvanostat instrument from Metrohm, controlled by the NOVA software (version 1.8, Ecochemie, Netherlands). For safety precautions, every CNS sample was stored in sealed petri dishes.

2.3 Cellular Tests

In order to prove biocompatibility, CNS samples were first sterilized by a 30-min incubation in 70% ethanol and subsequently biofunctionalized by incubating them for 30 min in PLL (500 µg/ml, prepared in borate buffer, pH 8). Hippocampal neurons were isolated from 17-day-old FVB mouse embryos as described previously.[70] Therefore, time-pregnant mice were euthanized and embryos removed. After decapitation of the embryos, the brains were removed and the hippocampi were dissected from the cerebral hemispheres. After being incubated in 0.05% trypsin-EDTA for 10 min in an incubator at 37°C and 5% CO_2 atmosphere, the hippocampi were washed three times with Hanks Balanced Salt Solution (HBSS without Ca^{2+} and Mg^{2+}, Invitrogen, Belgium). Fire-polished Pasteur pipettes with different tip sizes were used to mechanically dissociate individual cells in HBSS. Next, the cells were centrifuged at 1000 rpm for 5 min to discard supernatant and subsequently resuspended in MEM horse medium. Approximately 70 000 cells/cm^2 were plated on a CNS substrate of 2 cm^2 in Neurobasal medium containing 12.5 mM glutamate and B27 supplement (Invitrogen). After three days of plating the medium was changed to Neurobasal medium without glutamate, and 5µM cytosine arabinoside (Ara-C) was added to inhibit the proliferation of glial cells. After five days of plating the cells were taken out of the incubator and examined using an apoptosis kit (Vybrant apoptosis kit, Invitrogen). Fluorescent pictures were taken using a CellR (Olympus) set-up equipped with a BX51-WI microscope. As a reference, primary hippocampal neurons were cultured on PLL-coated glass coverslips.

2.4 Statistical Analysis

Statistical analysis was performed using the Graphpad Prism 5 Software (Graphpad Software Inc., California, USA). A Grubbs' test ($\alpha = 0.05$) was used to determine the outliers which were excluded from the

data. Normality of the data was examined by means of a D'Agostino-Pearson omnibus normality test. A student t-test was used to compare two groups in case of a Gaussian distribution. Multiple groups were compared using a one way analysis of variance (or one-way ANOVA) technique and a Tukey's multiple comparison post-hoc test. When the data was not following the Gaussian distribution a Wilcoxon rank-sum test was performed to compare two groups. A Kruskal-Wallis ANOVA test was applied with a Dunn's post-hoc test to compare multiple groups. Statistical significance was reached at p-values ≤ 0.05.

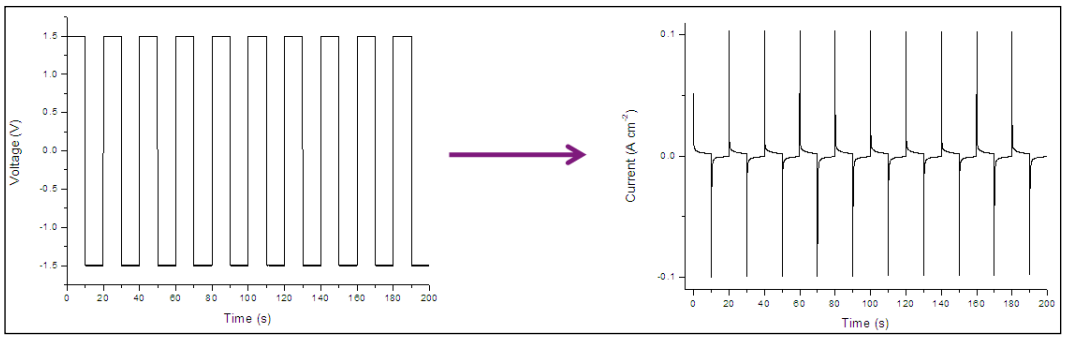

Fig. 6. The application of 10 s biphasic voltage pulses from +1.5 to -1.5 V yields a corresponding current. By integrating and summing the positive parts of this current graph, the total charge density delivered at the anodic phase can be calculated.

3. Results

3.1 (Electrochemical) Characterization of Pristine CNSs

Untreated CNSs were electrochemically characterized using CV profiling and EIS measurements. Initially, two different underlayer substrates were investigated, i.e. a 300 nm layer of aSi or TiN. Adherence on both materials was assessed by a simple Scotch tape adherence test, followed by the electrochemical experiments which allow for the calculation of the CSC_c, impedance and CPE.

3.1.1 TiN vs aSi Underlayer Substrates

One first important observation that was made was the clear difference in adhesion of the CNSs grown on aSi and TiN substrates. While the CNSs grown on TiN demonstrated good adherence and robustness, the CNSs on the aSi substrates were very fragile and tended to detach from the surface very easily. For this reason, a simple Scotch tape test was performed to probe the adhesion strength of the sheets. The results, shown in the supplemental **Fig. S1**, indicated two important points, namely: (i) that there is a clear difference in CNS adhesion between aSi and TiN substrates, and (ii) that the adhesion strength is also dependent from where the sample was acquired; i.e. the center or edge region of the wafer. For aSi substrates, CNSs grown on the edge of the wafer completely detached from the surface, while the center region demonstrated better adherence of CNSs; here only a small percentage was transferred to the tape. In contrast, CNSs deposited on TiN substrates were very robust and the tape was not able to detach any sheets from neither the center nor the edge of the TiN wafer. For these and other reasons described in the next section, further research on CNSs was conducted with TiN substrates.

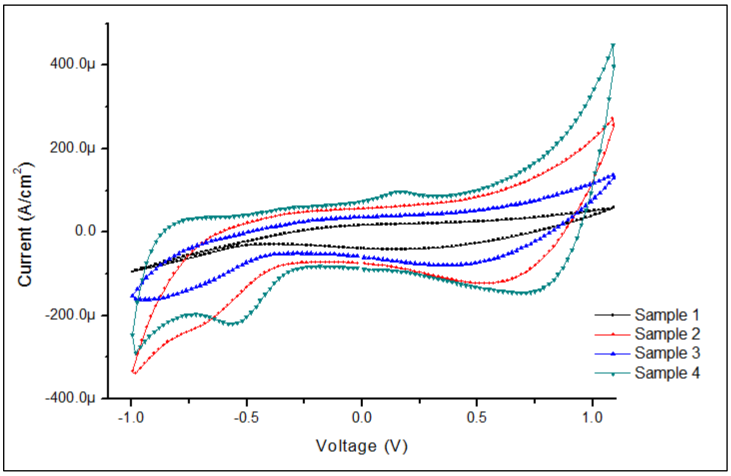

Fig. 7. Cyclic voltammograms of four samples of CNSs grown on aSi substrates. Samples 1-3 were acquired from the edge of the wafer and show a high degree of variation. Sample 4 originated from the center of the wafer and displayed a more ψǘèLJƛŎl·ȶΩ CNS cyclic voltammogram.

Fig. 7 shows four independent cyclic voltammograms of methane-based CNSs deposited on aSi substrates. Although they all originated from the same wafer, the samples show a large degree of variation with no clear voltage-current relationship. The only sample that resembled a 'typical' CV curve of CNSs is sample 4, which originated from the center of the wafer. The other three samples were acquired from the wafers' edge. These results imply that the electrochemical properties of CNSs on aSi substrates are highly variable, and that aSi is therefore not a suitable material to support CNS electrodes. These results were double-checked to ensure reliability.

3.1.2 Methane-based CNSs Deposited on TiN

The electrochemical characteristics of methane-based CNSs deposited on 300 nm TiN substrates were investigated. A visual inspection of the wafer revealed a clear color gradient from deep black at the edge to reflective metallic at the center. This observation already suggested that, just like CNSs grown on aSi, the electrochemical properties would differ depending on which part of the wafer is measured. The results, shown in **Fig. 8(a,b)**, clearly show a difference in electrochemical behavior depending on location; CSC_c values were approximately 0.14 ± 0.008 and 0.24 ± 0.001 mC cm^{-2} for the wafers' center and edge respectively ($P<0.01$). Also a difference in impedance was found in the capacitive part (the increasing part of the graph starting at approximately 100 Hz) of **Fig. 8(c)**. It is in this low-frequency region where double-layer capacitance effects become increasingly dominant. Impedance values at 0.1 Hz were 23.40 ± 1.89 and 9.64 ± 0.13 kΩ for the center and edge of the wafer respectively. Also at 1 kHz (the frequency scale for neuronal APs and thus the frequency by which electrodes are usually characterized [32]), the impedance was slightly lower at the edge (19.21 ± 2.34 Ω) than at the center (32.18 ± 6.82 Ω). Also CPE values were proven to be higher for the edge region of the wafer (**Fig. 8(d)**; $P<0.01$). It is, however, important to note that the surface area of these CNS samples is very large, especially when compared to the patterned, micron-sized electrodes that are used in typical stimulation and recording experiments with MEAs. The impedance values in the high-frequency regime (here between 100 Hz to 100 kHz) are therefore not really representative. Elementally, a decrease in electrode size automatically leads to a corresponding increase in impedance, which means that the graph of Fig. 8(c) will shift to the right. Hence, the impedance measured in the high-frequency regime represents essentially the resistance of the solution. This should be kept in mind throughout any further electrochemical experiments described in the next sections.

The sharp current increases at the end of the cathodic and anodic scans of the cyclic voltammogram of Fig. 8(a) are due to the onset of H_2 and O_2 gas evolution, respectively. The reductive and oxidative peaks between 0-0.2 V originate from the reduction and subsequent oxidation of dissolved O_2. Also a well-defined reductive peak near -0.5 V and an only ill-defined broad oxidation band between -0.5 V and -0.2 V can be observed. These peaks can be attributed to H adsorption and desorption.

Fig. 9 shows XSEM micrographs of CNSs deposited on both wafer positions. It was found that the length of the CNSs at the edge was approximately two times the length of CNSs deposited at the center (170 vs.

380 nm respectively), which provides an explanation for the observed differences in electrochemical behavior, as well as the observed color gradient of the wafer.

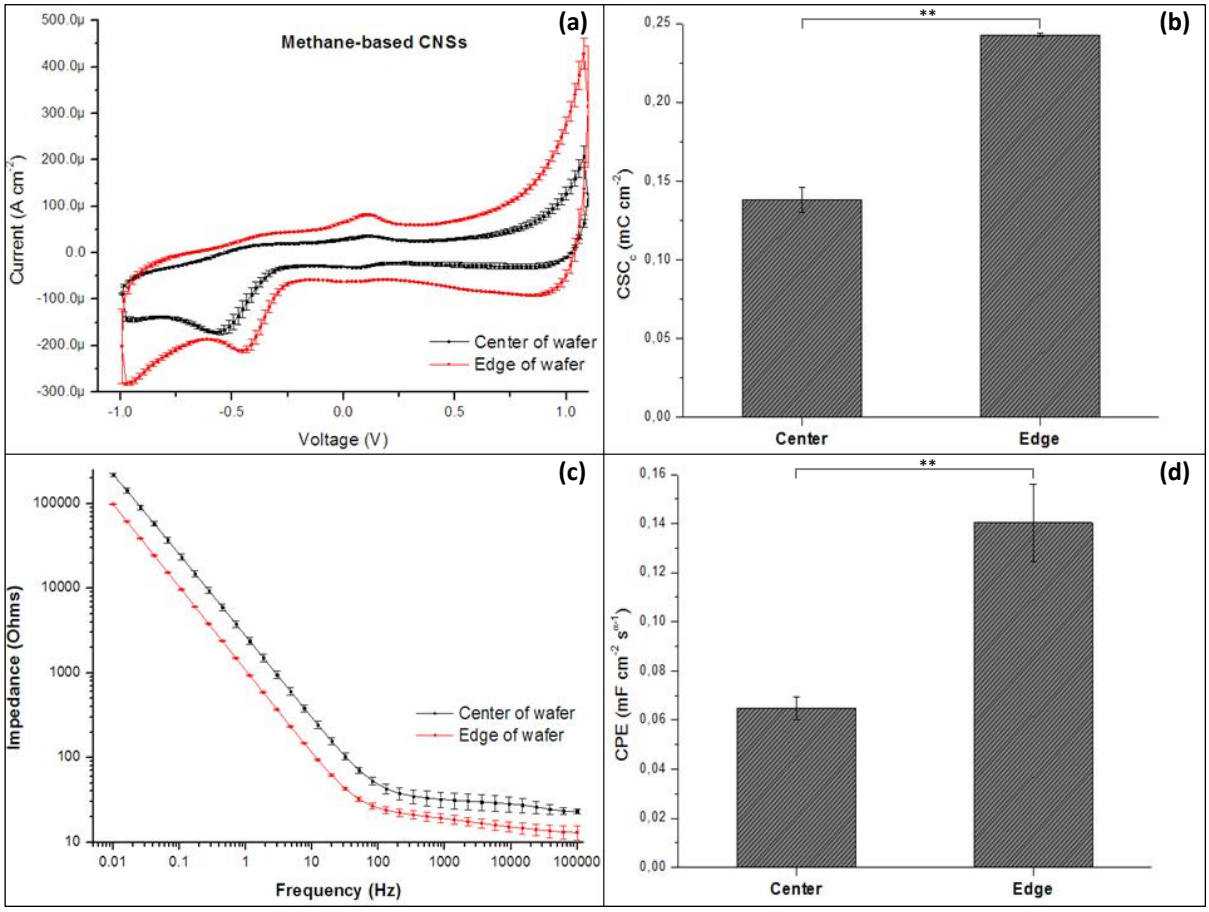

*Fig. 8. (a) Comparative CV curves of methane-based CNS samples originating from the center (n=8) and edge (n=11) of the TiN wafer. Samples obtained from the edge of the wafer demonstrated (b) higher CSC_c values, (c) lower overall impedance and (d) higher CPE values. **P<0.01*

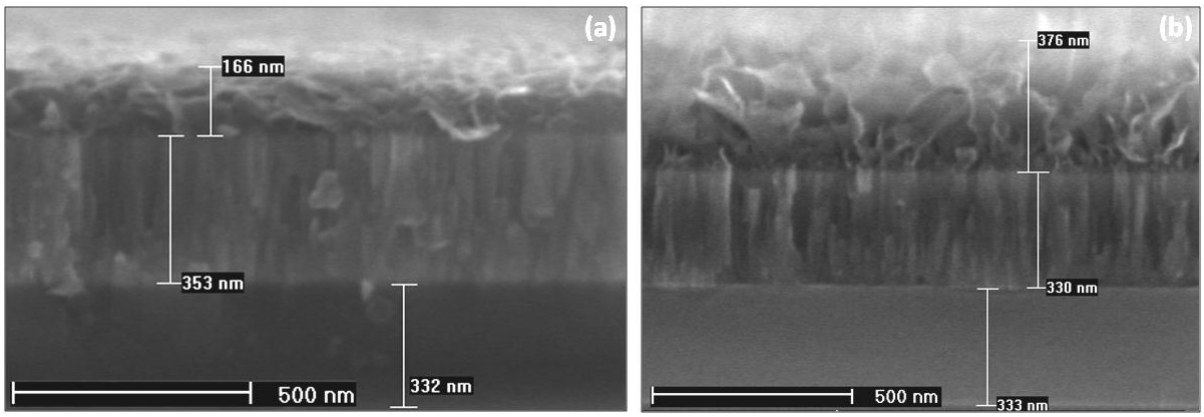

Fig. 9. Cross-sectional SEM picture of methane-based CNSs deposited on (a) the center and (b) the edge of the wafer. Average CNS lengths were approximately 170 and 380 nm respectively. The layer underneath the CNSs is TiN, whereas the bottom region of the wafer consists of SiO_2.

3.1.3 Acetylene-based CNSs Deposited on TiN

Fig. 10 shows the electrochemical characteristics of acetylene-based CNSs grown on 300 nm TiN substrates. As with the methane-based CNSs, differences were again found between the center and edge of the wafer. Also here the edge regions demonstrated better electrochemical properties than the center area; CSC_c values were 0.50 ± 0.04 and 0.32 ± 0.018 mC cm^{-2} respectively (P<0.01). These results are higher than the ones obtained for the methane-based CNSs (comparison **Fig. 10(b)**; P<0.001). Also the impedance in the capacitive region proved to be slightly lower for CNSs grown with the acetylene precursor gas; values at 0.1 Hz were 5.3 ± 0.23 and 3.8 ± 0.38 kΩ for the center and edge respectively (**Fig. 10(c)**). The observed peaks in the cyclic voltammograms were identical to the ones described in the previous section.

Also here XSEM investigation revealed differences in length of acetylene-based CNSs depending on their position (**Fig. 11**). The length of the CNSs at the edge of the wafer was approximately three times larger than the length of CNSs at the center region (460 nm vs. 1.3 µm respectively). As the length of these acetylene-based CNSs is several orders of magnitude greater than the methane-grown ones examined in the previous section, no ideal comparisons can be made between their intrinsic electrochemical properties, i.e. if the higher experimental results are mainly due to their difference in length. However, it was found that when an

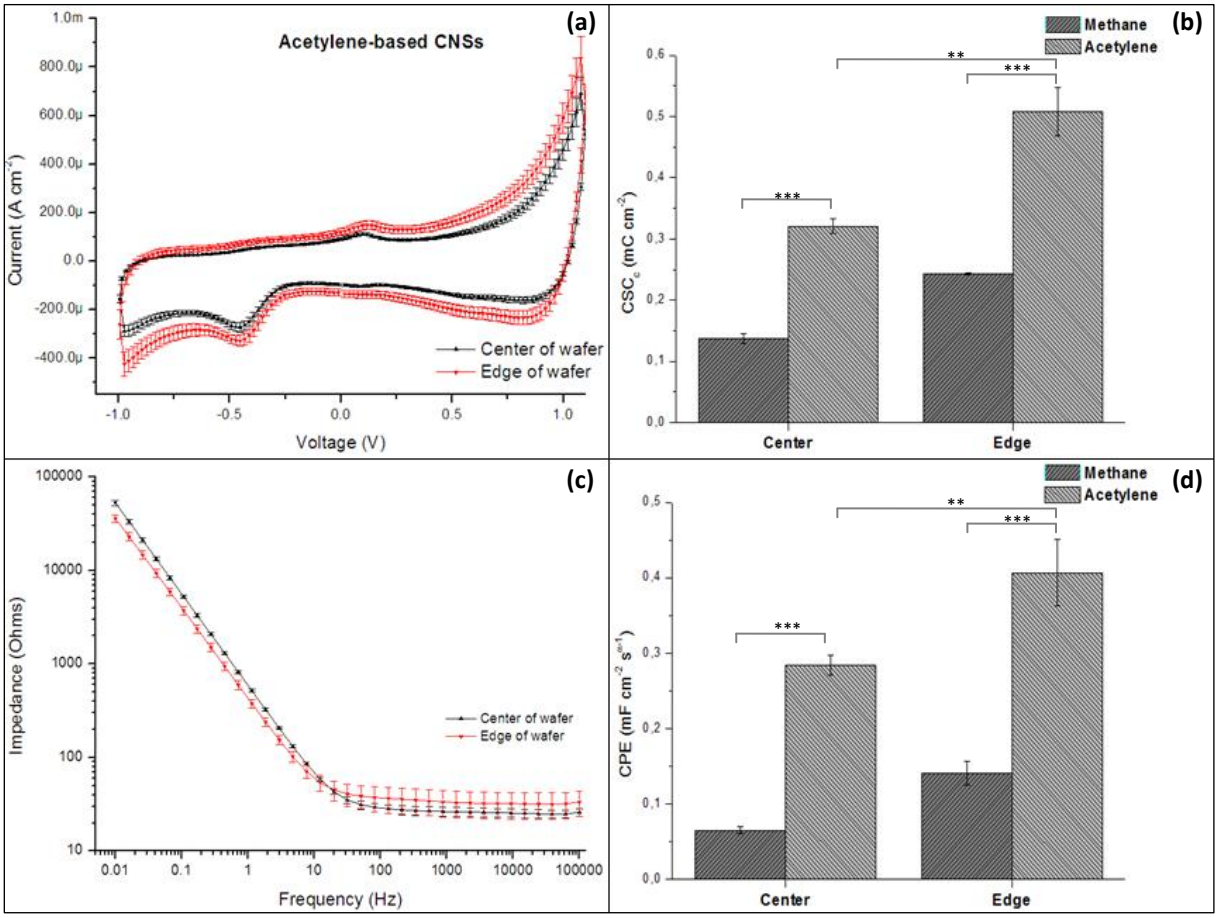

*Fig. 10. (a) Comparative CV curves of acetylene-based CNS samples originating from the center (n=9) and edge (n=11) of the TiN wafer. (b) Comparison of the CSC_c of methane and acetylene-based samples. Acetylene-grown CNSs obtained from the edge of the wafer demonstrated the highest CSC_c, (c) lower overall impedance and (d) highest CPE values. **P<0.01; ***P<0.001*

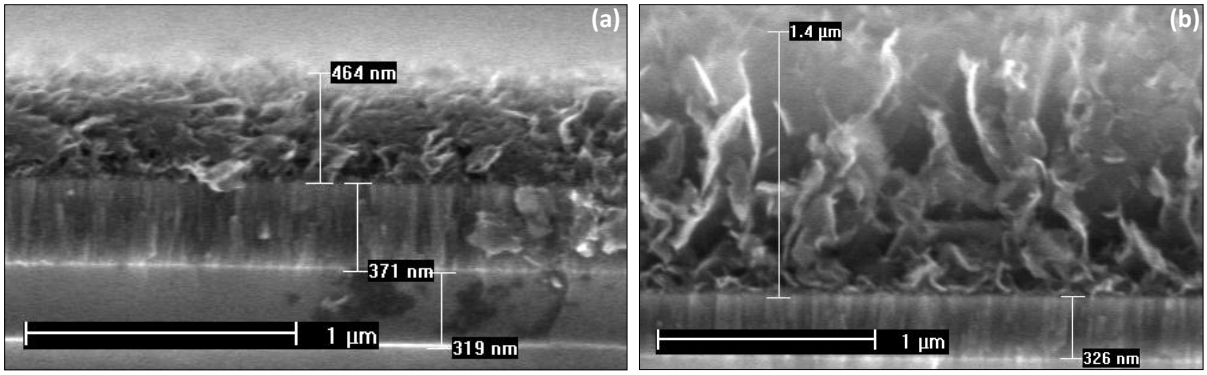

Fig. 11. Cross-sectional SEM picture of acetylene-based CNSs deposited on (a) the center and (b) the edge of the wafer. Average CNS lengths were approximately 460 nm and 1.3 µm respectively.

acetylene precursor gas was used for the CNS growth process, CNSs became much thicker with a more branched, tree-like structure (and thus more 'defective', i.e. a higher concentration of graphitic edges). Moreover, further research on growth conditions showed that, for both types of CNSs, the edge region of the wafer possesses a higher amount of long CNSs with a relatively thin base, while CNSs grown at the center region are short and thick at their base. A schematic illustration of this can be found in the supplemental **Fig. S2**.

Generally, these initial experiments confirm that samples of CNSs, grown on TiN substrates, exhibit different electrochemical properties dependent upon the precursor gas used and their location on the wafer. Compared to methane, an acetylene precursor gas yields longer, thicker and more branched CNSs. Samples from the wafers' edge are demonstrate higher CSC_c and lower impedance values, and are therefore better suited to use as an electrode material than samples with CNSs that are deposited at the center of the wafer.

3.2 Effect of UV/O_3 Treatment

Both types of CNSs deposited on TiN substrates were treated with UV/O_3 in order to increase wettability and to investigate the effect on CSC_c, capacitance and impedance. UV/O_3 is a relatively straightforward and easy (dry-oxidation) process to functionalize the surface of the CNSs with oxygenated functional groups, which facilitates the formation of hydrogen bonds between the water molecules and CNS surface. Briefly, the UV radiation attacks the graphitic edges and sidewalls of the CNSs and allows the ozone to subsequently oxidize the surface. The results, shown in **Fig. 12**, show that even prolonged UV/O_3 treatments of up to 60 minutes can increase the CSC_c of CNSs by a factor of 3 to 4. Also the CPE values increased in a similar manner. The highest CSC_c and CPE values (1.45 ± 0.08 mC cm^{-2} and 2.60 ± 0.13 mF cm^{-2} $s^{\alpha-1}$ respectively) were found for the longer and more branched, acetylene-based CNSs; the edge samples yielding higher results than the ones originating from the center. Also, the UV/O_3 treatment decreased the impedance in the capacitive region in an exponential manner (**Fig. 12(c,d)**). For methane-grown CNSs originating from the center of the wafer, 60 min of UV/O_3 exponentially decreased the impedance by more than 90% (from 23.4 ± 1.89 kΩ to 1.66

± 0.09 kΩ at 0.1 Hz). The intrinsic impedance of the longer, acetylene-based CNSs at the edge is much lower (3.75 ± 0.38 kΩ), and a 60 min UV/O_3 treatment was able to further reduce the 0.1 Hz impedance to 0.56 ± 0.03 kΩ (-85%). In case of the methane-based CNSs, UV/O_3 exposure times longer than 60 min yielded no significantly better results and caused apparent damage to the samples. Static contact angle measurements revealed that even one minute of UV/O_3 was enough to lower the contact angle of the CNSs from approximately 125° to about 63°. Ten minutes of UV/O_3 allowed almost complete wetting of the surface, with a mean contact angle of approximately 8° (supplemental **Fig. S3**).

Although this is an excellent method to increase the capacitance of the electrodes, while at the same time significantly lowering their impedance, UV/O_3 is also quite destructive to the CNSs as it removes the carbon 'contaminants' to create volatile organics (such as CO and CO_2 molecules) during the desorption process. In other words, prolonged UV/O_3 exposure etches away the CNSs, as can be seen in the supplemental **Fig. S4**. UV/O_3 exposure times ranging up to 40 min caused no apparent structural damage to the (methane-based) CNSs, whereas 60-80 min of UV/O_3 removed their graphitic edges, leaving only a thin layer of carbon on the TiN surface.

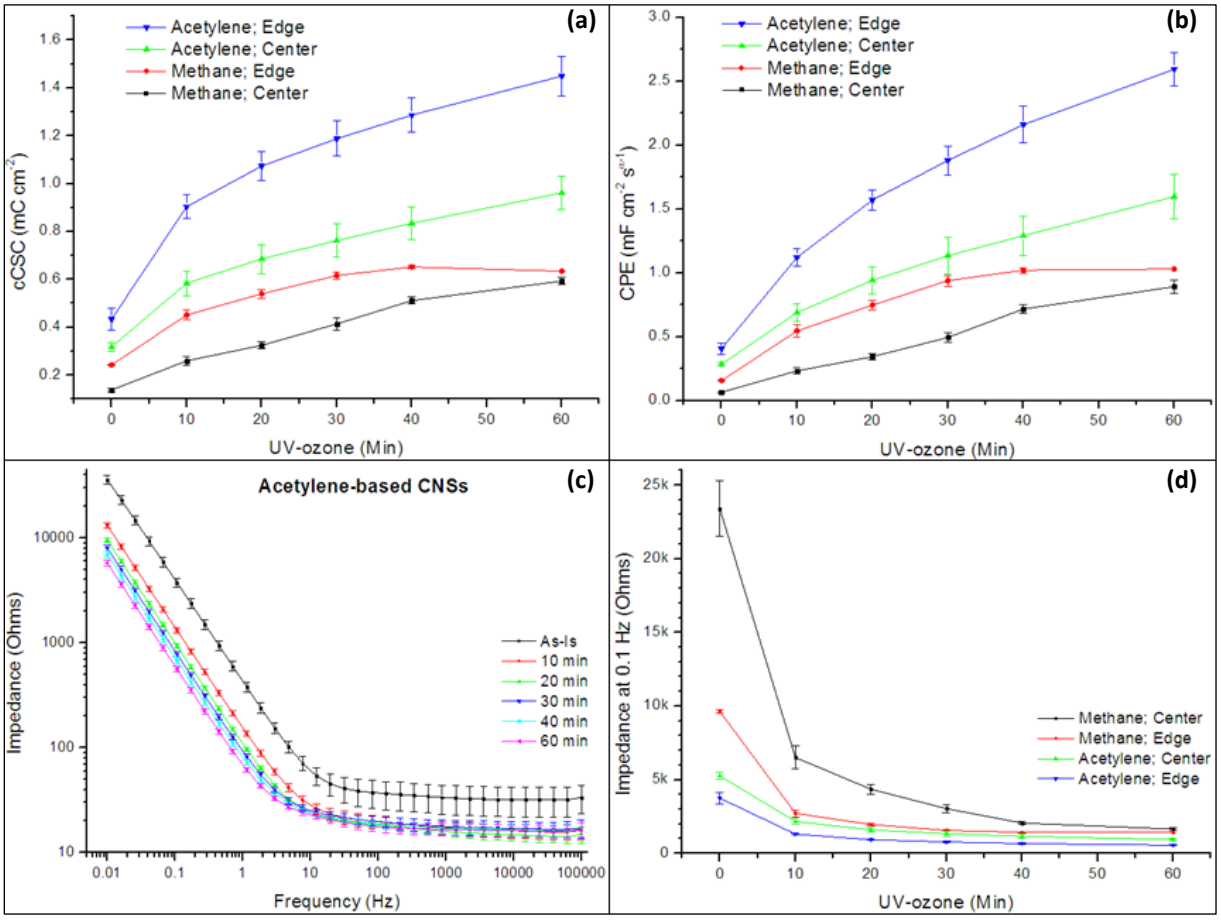

Fig. 12. Calculated (a) CSC_c and (b) CPE values for both methane as acetylene-based CNSs in function of the UV/O_3 exposure time. (c) Impedance results for the acetylene-grown CNS edge samples. (d) Comparative impedance results at 0.1 Hz.

Finally, UV/O_3 treated samples (50 min) were stored for up to two months in ambient conditions to investigate the effect of aging on CSC_c and impedance. Over a two month period the CSC_c decreased in an exponential manner (approximately -15%) but stabilized after four weeks. The impedance seemed to increase gradually but the difference after two months was found to be insignificant. In general, the outcome of this experiment was very similar to when pristine CNSs were stored in ambient air conditions (see section 3.4.1).

3.3 Effect of Voltage-Biasing

Apart from UV/O_3, another method to increase the electrochemical properties of CNSs is by applying an electric voltage bias. Voltage-biasing is a powerful yet nondestructive way to electrochemically oxidize the CNSs and to cause a transition from the hydrophobic to the hydrophilic state.[71, 72] Here, 10 s biphasic voltage pulses from ±1 V, ±1.25 V, ±1.5 V and ±2 V were applied to the samples respectively. Generally, for both methane (results not shown) and acetylene-based CNSs, voltage-biasing with 1 V had only a minimal effect on the CSC_c and impedance; **Fig. 13(a)** shows that after 100 pulses (corresponding to an accumulated charge density of 1.1 C cm^{-2} ph^{-1}) the CSC_c merely rose to 0.77 mC cm^{-2}. When the voltage was increased to 1.25 V and 1.5 V, both the total charge density as CSC_c increased dramatically, the highest CSC_c value being 2.16 ± 0.01 mC cm^{-2} at a total charge density of 2.5 C cm^{-2} ph^{-1} (or 60 pulses) for 1.5V (**Fig. 13(b)**). After this point, a further increase of the total charge density resulted in a slow but steady decrement of the CSC_c and detachment of the acetylene-based CNSs at the edge of the electrode. It was also observed that biasing with 1.25 V and higher resulted in the formation of fine gas bubbles at the electrodes, indicating that water was being electrolyzed. Compared to the Pt electrode, where the gas formation manifested itself by a continuous stream of bubbles, a gaseous sheath was formed by static bubbles on the CNSs electrodes. Lastly, a 2 V bias increased the accumulated charge density, but the maximum obtained CSC_c was lower than the CSC_c obtained for 1.5 V; approximately 1.85 ± 0.02 mC cm^{-2} (not shown in graph). Moreover, the electrodes were irreversibly damaged as the CNSs completely detached from the TiN substrate.

Fig. 13(c,d) shows that voltage-biasing with 1.5 V yields higher CSC_c and lower impedance values than the ones obtained for the UV/O_3 treatment. Although the saturation point of the CSC_c (and impedance) for UV/O_3 was not yet reached after 60 min, voltage-biasing yields apparent better electrochemical results. Moreover, compared to the rather destructive character of UV/O_3, this method has a less dramatic effect on the morphology and topography of the CNSs, as can be seen in **Fig. 14**. Here, 90 pulses of 1.5 V were given to the CNS electrodes, i.e. well beyond the CSC_c inflection point. Even though the electrode area showed a small change in color, the morphology changed only slightly; the CNSs appeared more wrinkled but maintained their flake-like structure and sharp edges. Based on these findings, we can reasonably expect that the morphology of the CNSs does not change significantly when only 60 pulses of 1.5 V are applied (i.e. a total charge density of 2.5 C cm^{-2} ph^{-1}).

Lastly, the effect of aging was investigated. Carbon nanosheet samples were voltage-biased with 60

pulses of ±1.5V and stored in ambient conditions for two months. Over this two month period the CSC_c decreased in an exponential-like manner (approximately -20%) while the impedance did not change significantly; results which are comparable as when the CNSs were stored after a UV/O_3 treatment.

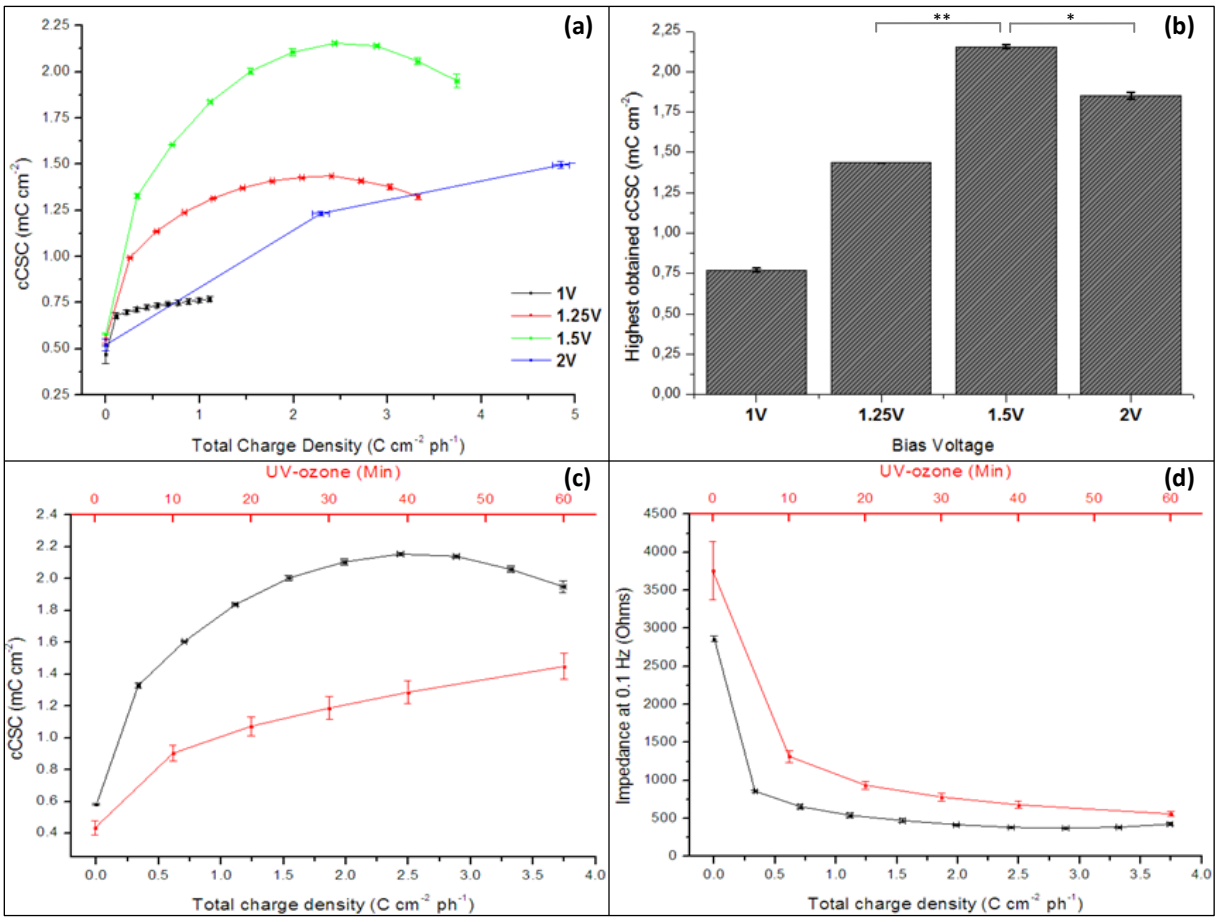

*Fig. 13. (a) CSC_c in function of the total charge density delivered to the electrodes and (b) the highest CSC_c that was obtained for each voltage. (c) Compared to a UV/O_3 treatment (red curve), voltage-biasing (black curve) yielded higher CSC_c results and (d) a lower impedance (here compared at 0.1 Hz). *P<0.05; **P<0.01*

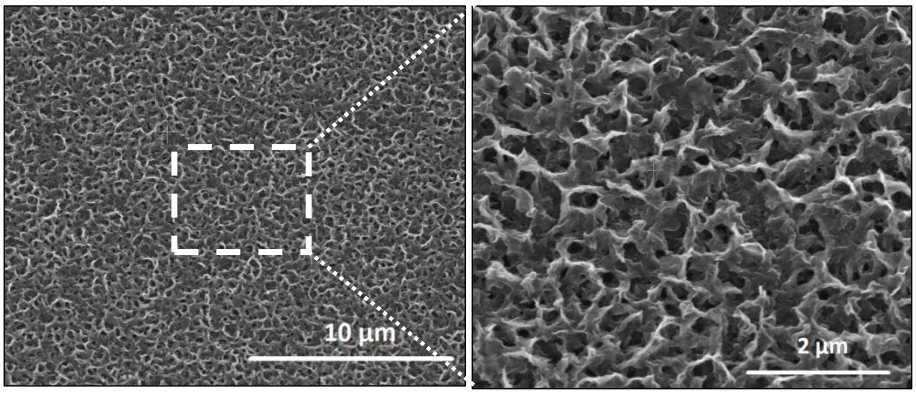

Fig. 14. SEM picture of the (acetylene-based) CNSs after voltage-biasing. Even 90 pulses of ±1.5V caused no considerable damage to the CNSs.

3.4 Storage in Dry and Liquid Conditions

As it is important to know if the electrochemical properties of CNSs change over time when they are stored in dry or liquid conditions, CNS stability in different media was investigated. Cyclic voltammetry and EIS experiments were performed on CNSs that were stored for two months and two weeks in ambient air conditions and liquid PBS, respectively.

3.4.1 Storage in Ambient Air Conditions

The electrochemical properties of pristine, as-grown CNSs were measured after one, two, four and eight weeks of storage in ambient air. **Fig. 15(a,b)** shows a considerable difference in the cyclic voltammograms of acetylene and methane-based CNSs after a storage period of two months. For both types of CNSs, the CSC_c decreased approximately 20% after eight weeks of air storage (**Fig. 15(c)**); from 0.55 ± 0.02 to 0.44 ± 0.01 mC cm^{-2} for the acetylene-based CNSs and from 0.27 ± 0.01 to 0.20 ± 0.003 mC cm^{-2} for the methane-based ones. This was accompanied by a corresponding increase of approximately 40% in impedance in the capacitive region (**Fig. 15(d)**); at 0.1 Hz the impedance for the acetylene-based CNSs rose from approximately 2.8 ± 0.08 to 4.8 ± 0.14 kΩ. After eight weeks the impedance of the methane-based CNSs increased from 8.1 ± 0.4 to 13.7 ± 0.6 kΩ. Similar results were found when the CNS electrodes were stored in N_2.

3.4.2 Storage in Liquid PBS

Phosphate buffered saline is one of the most commonly used buffers in biological research. The solution is non-toxic to cells and maintains their osmolarity (isotonic), while the phosphate groups in this buffer solution help to keep the pH at a constant level (7.4).[73] It is therefore of interest to study the effect of storing CNSs in a water-based, cell-friendly medium. The results, shown in **Fig. 16**, show no significant change in CSC_c when the CNSs are stored for up to two weeks in PBS. Also the impedance in the capacitive region remained unchanged. Only in the resistive region a small increase of impedance can be observed for both types of CNSs, which, as explained in the previous section, is probably due to the small differences in solution resistance.

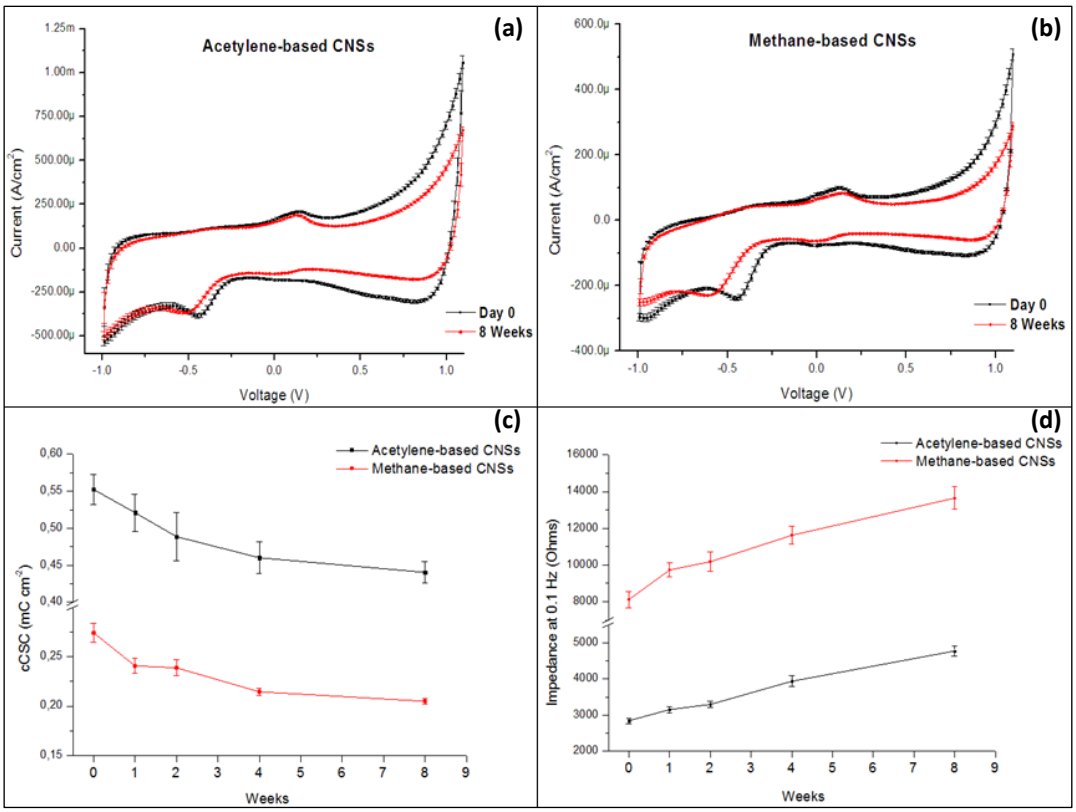

Fig. 15. Comparative cyclic voltammograms of (a) acetylene-based and (b) methane-based CNSs. The red curve corresponds to the electrochemical characteristics after 4 weeks of air storage, and lead to (c) a decrease in CSC_c and (d) an increase of impedance in the capacitive region (0.1 Hz).

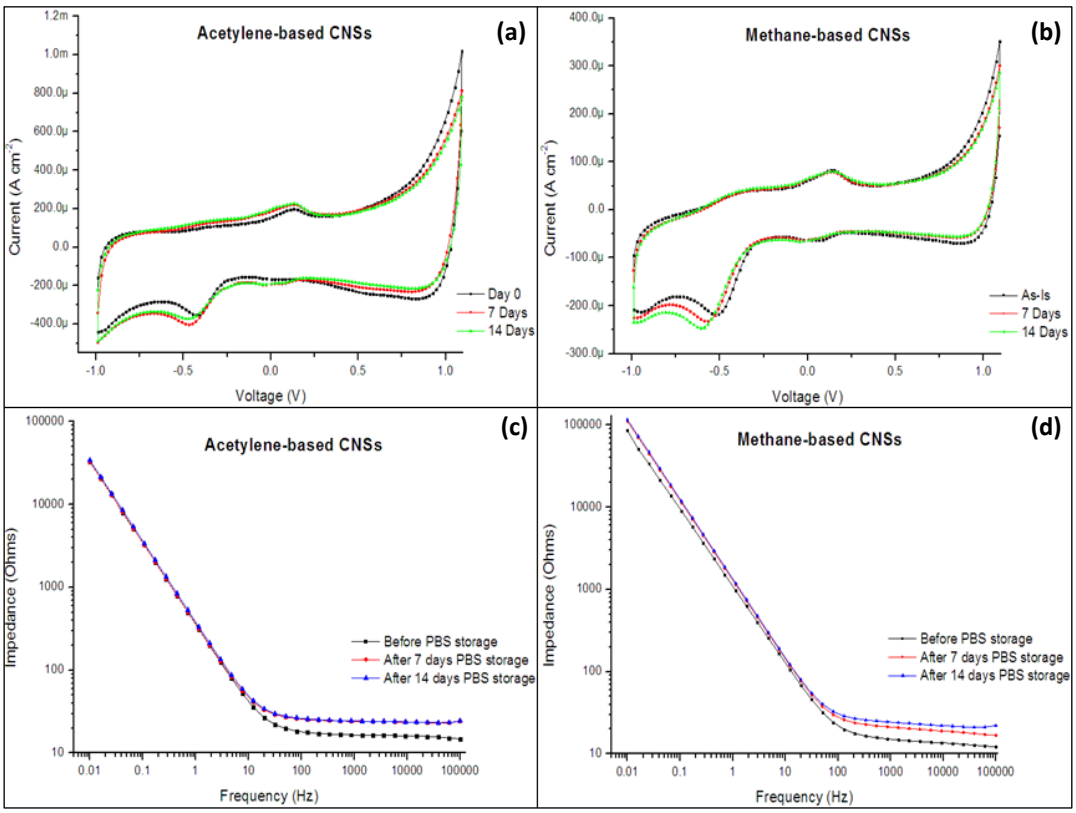

Fig. 16. Electrochemical properties of (a,c) acetylene-based CNSs and (b,d) methane-based CNSs when stored in PBS for up to 14 days.

3.5 CNS Biocompatibility

Primary mouse hippocampal neurons were cultured on both pristine and surface-treated acetylene-based CNSs. After five days in culture, the cells were stained with an acetomethoxy derivate of calcein (calcein AM) and propidium iodide (PI) and subsequently assessed for viability. Calcein AM is a fluorescein complex that is transported through the cellular membrane where it binds to intracellular Ca^{2+}, which results in a bright fluorescent signal. Intracellular enzymes (i.e. esterases) remove the acetomethoxy group of the molecule to assure that the calcein cannot leak back out of the cell.[74] Consequently, calcein AM only labels live cells that contain this active enzyme. Propidium iodide is a red fluorescent molecule which is impermeable to the membrane, and can therefore only stain necrotic or apoptotic cells (which display large holes in their membrane complex) by intercalating between the DNA base pairs.[75]

Fig. 17 shows that pristine CNSs, due to their intrinsic hydrophobic nature, do not support neuronal cell growth; cell viability was approximately 9% ± 9%. Surface treatments for making the CNSs hydrophilic are also not sufficient for the cells to grow; neither a UV/O_3 treatment (50 min; 16% ± 17%) nor voltage-biasing (70 pulses of ±1.5V; 3% ± 2%) of the CNSs was able to generate biocompatible substrates. In all of these cases, the few hippocampal neurons that could be observed were free-floating clumps of cells, most of which were either dead or apoptotic with no neurite extensions, an example of which can be seen in the supplemental **Fig. S5(a)**. The small fraction of cells in these clumps that were alive and stained green were responsible for the viability results described above. Thus, viability of neuronal cells on both pristine as surface-treated CNSs can essentially be considered to have a value close to 0%.

In order to increase cell adhesion the CNS samples were coated with poly-L-lysine (PLL); a widely used, positively charged polymer that improves cell adhesion by altering surface charges on the culture substrate.[76] Although viability between pristine CNSs en CNSs coated with PLL was found to be significantly different ($P<0.05$), neuronal growth was strongly concentrated on the PDMS layer that delimited the circular CNS area. Once cells reached this boundary line they clearly evaded the CNSs; cell growth came to a halt and neurites were projected either one way or the other along the demarcation line (**Fig. S5(b)**). On the CNSs themselves a high concentration of dead cells and some free-floating clumps were observed. The addition of PLL to pristine CNSs has therefore no effect on biocompatibility, and despite the significant difference that was found (due to cell growth on the PDMS), the viability can be considered to be the same as when the pristine samples are not coated with PLL. A more in-depth study with fluorescently (FITC-)labeled PLL revealed that PLL bound to the PDMS layer, but not to the CNSs (**Fig. S5(c)**). Better results were found with PLL-coated samples that underwent a prior UV/O_3 treatment or were voltage-biased; cell viability was 58% ± 18% and 74% ± 12% respectively, a difference which was found to be significant ($P<0.05$). Neuronal cells showed good adherence to the CNS substrates, with long and numerous neurites that extended in all directions. Also, in contrast to the pristine CNS samples, where cells mainly grew onto the PDMS layer after being coated with PLL, the neuronal cells were now preferably growing onto the CNS substrate. Compared to the reference (which had an average viability of 77% ± 7%), PLL-coated UV/O_3 samples showed a significantly lower cell viability ($P<0.05$), while no

significant difference was found between the reference and PLL-coated, voltage-biased CNSs.

Voltage-biased, PLL-coated CNSs are thus a good substrate to foster and promote both cell growth and survival. Although the UV/O_3 treated, PLL-coated CNSs yield significantly lower results, they also prove to be a useful and biocompatible substrate. From these viability experiments we can conclude that both a hydrophilic surface and an additional coating with adhesive proteins are required for neuronal cells to attach, grow and form elaborate neurites on CNSs. **Fig. 18** shows the fluorescent staining of calcein-AM and PI accumulated in the cells, seeded on the different CNS substrates.

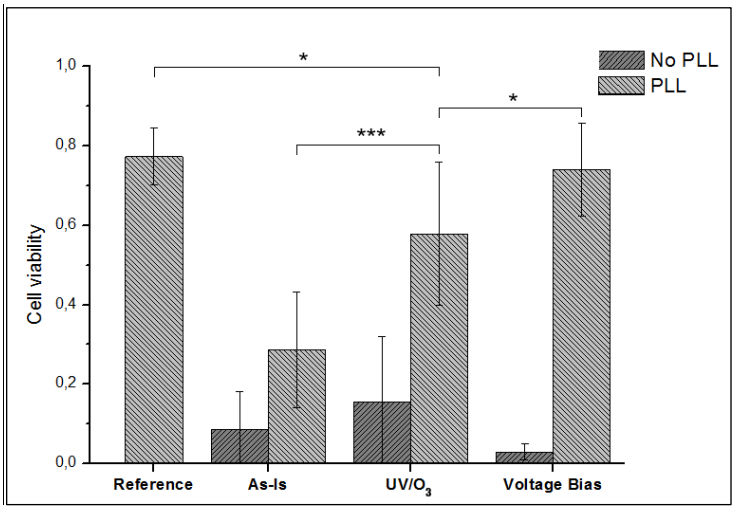

Table 1. Cell viability on both pristine and surface-treated CNSs, with and without a PLL coating.

	No PLL	PLL
Reference	/	0.77 ±0.07
As-Is	0.09 ±0.09	0.29 ±0.15
UV/O_3	0.16 ±0.17	0.58 ±0.18
Voltage Bias	0.03 ±0.02	0.74 ±0.12

*Fig. 17. Cell viability on differently treated CNS substrates. PLL-coated glass coverslips were used as a reference (n=8) and compared to pristine CNSs (as-is; n=10), pristine CNSs + PLL (n=7), UV/O_3 treated CNSs (n=13), UV/O_3 treated CNSs + PLL (n=13), voltage-biased CNSs (n=10) and voltage-biased, PLL-coated CNSs (n=14). Data are shown as mean (SD). *P<0.05; ***P<0.001.*

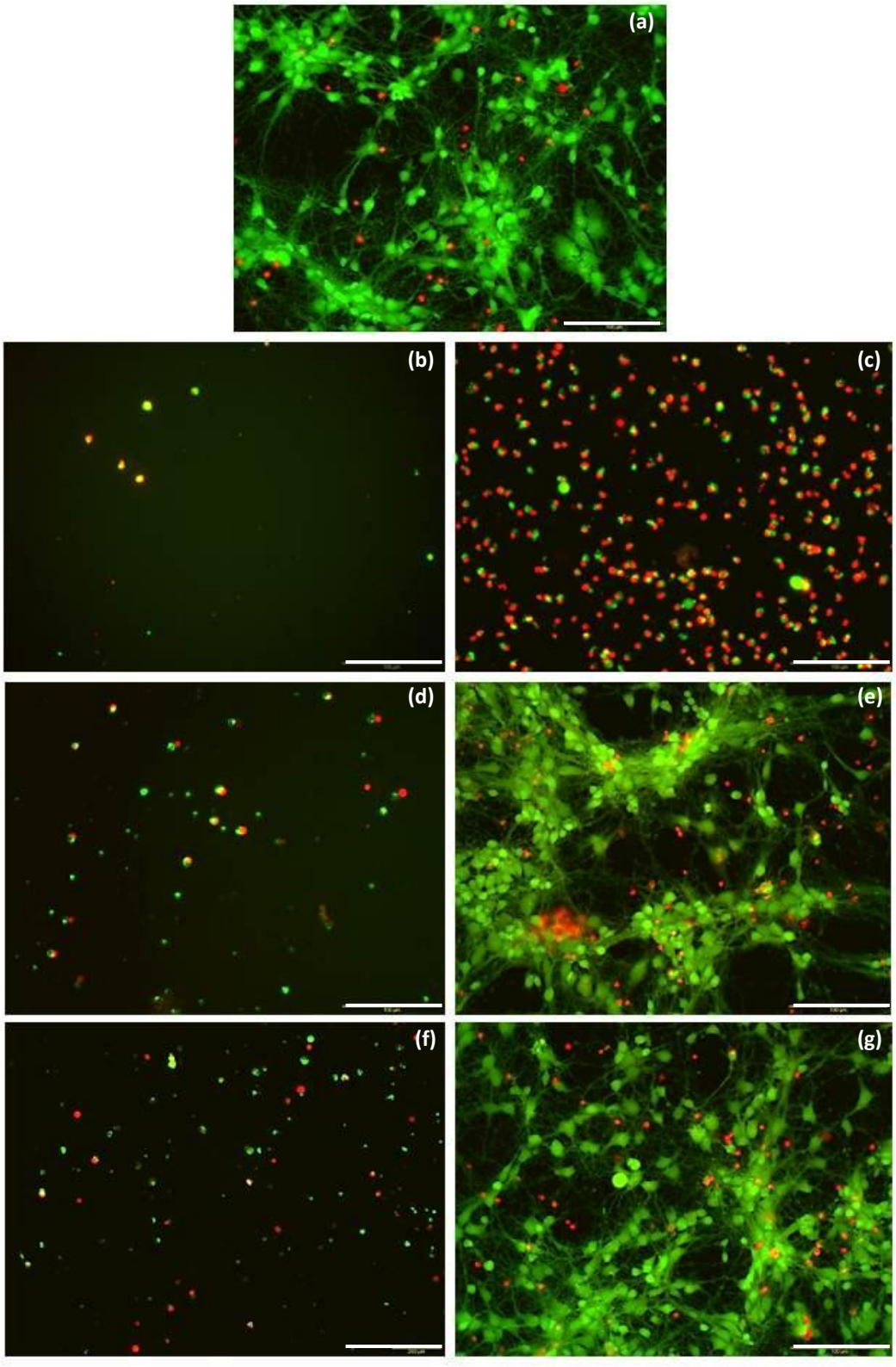

Fig. 18. Fluorescent images of the uptake of calcein-AM and PI by primary mouse hippocampal neurons seeded on different CNS substrates. (a) Reference. (b,d,f) Pristine, UV/O_3 treated and voltage-biased CNSs. (c,e,g) Pristine, UV/O_3 treated and voltage-biased CNSs coated with PLL. The scale bar corresponds to 100 µm.

4. Discussion

4.1 Intrinsic Properties of Methane and Acetylene-based CNSs

Using MPECVD, CNSs were deposited on 300 nm aSi and TiN substrates and subsequently compared for adhesion and electrochemical behavior. Whereas CNSs grown on TiN demonstrated strong adhesion and robustness, aSi did not prove to be a suitable substrate to support CNSs. Furthermore, differences in adhesion were found between the center and edge of the aSi wafer; especially the edge of the wafer showed very poor adhesion and highly variable electrochemical properties. We hypothesize that these last two parameters are, probably, correlated in a sense that weak chemical bonding between the CNSs and the substrate makes the electron movement less effective and more variable. At the center of the aSi wafer, where CNS adhesion was much stronger, the results were also noticeably better.

In contrast to aSi, CNSs deposited on TiN wafers yielded very stable and reproducible results. The Scotch tape adhesion test was not able to detach any CNSs from the TiN substrate, which indicates very strong intermolecular bonding between the carbon and TiN lattice. But also here the edge and center of the wafer rendered different electrochemical performances. Generally, for both methane and acetylene-based CNSs, the wafers' edge yielded better results than the center, with the acetylene-based CNSs demonstrating the best electrochemical properties. As already briefly explained in the previous section, when methane is used as the precursor gas, the resulting CNSs are thin and relatively unbranched. In contrast, acetylene yields thicker, more branched (and thus more defective) CNSs (supplemental **Fig. S2**). Because of their thicker base, they can be thought of as a variation on the so-called carbon nanowalls.[77, 78] Only here the CNS growth process makes the structures more branched which increases their effective surface area. Although more research should be performed on the specific impact of CNS length, we can already make some generic remarks about the parameters that primarily determine their electrochemical behavior. The specific surface area is correlated with both CNS length as well as their degree of branching. The increment of these two variables automatically leads to an increase in surface area, and thus a higher concentration of highly reactive graphitic edges. The rate of electron transfer should therefore be considerably larger with CNSs that are long and highly branched. Based on these assumptions, we can give a causal explanation of why acetylene-based, edge-deposited CNSs yield the highest electrochemical results. In these experiments, the difference in CSC_c between methane-based and acetylene-based edge CNSs was found to be approximately a factor of two. However, this cannot be fully attributed to the difference in precursor gas alone as the length of the compared CNSs was not identical. Nevertheless, as the height between the methane-based edge and acetylene-based center CNSs was approximately the same, we can reasonably state that the highly-branched, acetylene-based CNSs generally yield a higher CSC_c and lower impedance than methane-based CNSs.

4.2 UV/O_3 Treatment & Voltage-Biasing

Carbon nanosheets were exposed to a UV/O_3 treatment to functionalize the surface with oxygenated functional groups and thus to increase wettability and electrochemical characteristics. It was shown that UV/O_3 improves the interfacial properties between the electrolyte and CNSs; exposure times of up to 60 min were able to increase the CSC_c of acetylene-based CNSs from approximately 0.43 to 1.5 mC cm^{-2} (+250%). Furthermore, UV/O_3 exposure was able to reduce the impedance in the capacitive region by approximately 90%. It should be noted, however, that the duration of the UV/O_3 exposure is closely related to the CNS surface area. For instance, the short, methane-based CNSs started to reach a saturation point in CSC_c after 60 min of UV/O_3, whereas the saturation point of the longer, more branched acetylene-based CNSs was clearly not reached after the same amount of time (see Fig. 12(a)). Generally, these results imply that after an exposure time of roughly 60 min the CNSs will be virtually completely covered with oxygenated functional groups, which facilitates the formation of hydrogen bonds (and thus electron transfer) between the CNSs and surrounding water molecules. [21, 79]

Ten minutes of UV/O_3 was sufficient to lower the contact angle from approximately 125° to 8°, i.e. from hydrophobic to nearly superhydrophilic. This superhydrophilicity greatly enhances the double-layer capacitance of the CNSs, as protons in the surrounding liquid can approach the CNS surface much more easily, which consequently results in a better electron transfer.[21, 79] In other words, the UV/O_3 treatment increases the effective area of the Helmholtz layer, as the effective surface area between the CNSs and electrolyte is also increased. [21, 79] In contrast, when the samples are left untreated and the interface between these two remains (super)hydrophobic, electron transfer is considerably inhibited because of an interfacial thin film of air (even visible with the naked eye).[80] The electric double layer capacitance is thus directly related to the hydrophilicity in aqueous electrolyte systems.[79, 80]

One disadvantage of prolonged UV/O_3 irradiation is that it is detrimental for the carbon nanostructures. The energy of the UV photons is sufficiently high to alter the chemical bonds between the carbon atoms, and makes it possible to functionalize the CNSs with oxygenated functional groups. However, the UV/O_3 treatment is also capable of removing the carbon atoms to form volatile organic compounds (e.g. CO and CO_2). It is therefore of high importance to choose a UV/O_3 exposure time that is sufficiently long to adequately functionalize the CNSs with oxygen-containing functional groups, while simultaneously avoiding excessive etching damage. As stated above, the precise amount of time is primarily dependent on the length of the CNSs. From the experiments presented here, we can state that the UV/O_3 exposure time should not exceed 60 min for CNSs that are approximately 0.4 - 1 µm in height.

The introduction of various functional groups on the CNS surface can thus increase the double layer capacitance, which is predominantly determined by the materials' hydrophilicity; the easier protons in the electrolyte solution can reach the surface of the CNSs, the easier an electric double layer can form through non-faradaic processes.[21, 79] Apart from UV/O_3 exposure, voltage-biasing is another method to increase the materials' electrochemical properties. Of the several voltages tested between 1-2 V, voltage-biasing the CNSs with 1.5 V was able to generate higher CSC_c and lower impedance results compared to UV/O_3. The mechanism

responsible for the observed results is mainly attributed to the irreversible electrochemical oxidation of the CNSs due to the presence of water electrolysis, i.e. the reduction of water to hydrogen and oxygen.[81] This overall reaction can be written as:

$$2\ H_2O\ (l) \rightarrow 2\ H_2\ (g) + O_2\ (g) \qquad [3]$$

which can also be written as the sum of two half-reactions of the total water redox reaction:

$$2\ H_2O\ (l) + 2\ e^- \rightarrow H_2\ (g) + 2\ OH^-\ (aq) \qquad \text{(Cathodal reduction; } E_1 = -0.83V) \qquad [4]$$

$$4\ OH^-\ (aq) \rightarrow O_2\ (g) + 2\ H_2O\ (l) + 4\ e^- \qquad \text{(Anodal oxidation; } E_2 = -0.40V) \qquad [5]$$

The minimum voltage needed for electrolysis to occur is thus $E = E_1 + E_2 = -0.83V + (-0.40V) = -1.23V$. In other words, during the electrolysis of water hydrogen gas is produced at the cathode while oxygen gas is produced at the anode. An important mechanism that must be taken into consideration is the electrostatic adsorption of these two gases on the CNS surface (electrosorption). For example, graphite electrodes and carbon nanostructures have been shown to have a large adsorption capacity for hydrogen[81-83], the latter which have attracted significant interest in the field of hydrogen storage.[84-86] Especially graphene nanosheets are considered as a very promising candidate as hydrogen can diffuse into the interlayer space (i.e. intercalate/insert between the individual sheets).[86] The adsorption capacity for oxygen is smaller but substantial.[87, 88]

These features can, to a certain extent, explain the increase in electrochemical performance of voltage-biased CNSs. Based on the cyclic voltammograms, the electrochemical potential window (or water window) of the CNSs ranges from approximately -1 V to +1 V. Therefore, the application of ±1 V barely lead to the formation of oxygen or hydrogen gas at the electrodes. In contrast, when the potential window was crossed from -1.25 V to +1.25 V, the CSC_c increased dramatically (~200% after a total charge density of 2.5 C cm^{-2} ph^{-1}). Biasing with ±1.5 V led to an even higher CSC_c (~330% increase after the same amount of total charge density). Both at ±1.25 V and ±1.5 V, fine bubbles were formed on the electrodes, indicating that the water was being electrolyzed. Compared to the CNS electrode, where the bubbles were static and a gaseous sheath was developing over the surface, the Pt electrode produced a continuous stream of fine gas bubbles. This stream of gas was more profound when the Pt electrode served as the cathode, which is expected according to the overall electrolysis reaction of water (i.e. twice as much hydrogen gas is produced as oxygen).

The observed gaseous sheath on the CNS electrode reflects the absorption of oxygen and hydrogen gas on the surface, depending on the phase of the voltage pulse. Both oxygen and hydrogen atoms increase the wettability of the CNS surface, and thus the effective surface area between the CNSs and electrolyte.[21, 79] As the adsorption capacity of the CNS electrode is much higher for hydrogen than for oxygen, it will mainly be the adsorbed hydrogen atoms that are responsible for the observed increase of electrochemical properties.[81-83] The higher CSC_c and lower impedance compared to UV/O_3 can also be explained in this way; compared to UV/O_3, where functionalization only happens at the surface of the CNSs, voltage-biasing not only leads to the adsorption of functional groups at the surface, but also in between the individual CNSs and interlayer space.[86] It is this higher concentration of wetting groups that leads to the better electrochemical properties.

Furthermore, XSEM investigation showed that voltage-biasing with 1.5 V had almost no effect on the morphological properties of the CNSs, while CNS (etching) damage is directly proportional to UV/O_3 duration.

Lastly, a ±2 V voltage bias of the CNS electrodes rendered a lower CSC_c compared to the ±1.5 V bias. Together with the apparent damage and detachment of the CNSs, this voltage was evidently too high for the purpose intended here.

4.3 Storage of CNSs

Carbon nanosheets were stored in both dry and liquid conditions. After being stored for eight weeks in ambient air conditions, the CNS electrodes lost approximately 20% of their initial CSC_c, while the impedance rose approximately 40%. Similar aging experiments in ambient conditions have already been performed with CNTs, where it was hypothesized that CNTs are meta-stable materials (i.e. that CNTs are in a pseudo-thermodynamic equilibrium) that become more thermodynamically stable when they interact with pristine ambient conditions.[89] In this study, several unrelated properties such as surface area and pore volume, surface oxygen, and structural defects all decreased with 24 months of aging (fixed values after 12-15 months of aging). We hypothesize that similar mechanisms are responsible for the decreasing electrochemical properties of aging CNSs. Due to their highly reactive graphitic edges, freshly grown CNSs can be considered to be in a highly meta-stable state.[90] During the aging process, the concentration of structural defects decreases and the CNSs gradually become more thermodynamically stable. Furthermore, the exponential-like CSC_c curves indicate that, after a certain amount of time, the properties will stabilize and become fixed (as was the case for the CNTs). Further examination with X-ray photoelectron spectroscopy and Raman spectroscopy should verify if these phenomena are truly responsible for the observed decrease in electrochemical properties over time.

Because of their high intrinsic hydrophobicity, a small sheet of air is constantly trapped between the CNSs, which is clearly visible when they are submerged in water. In contrast, when the CNSs are made more hydrophilic after a voltage-bias or UV/O_3 treatment, this interfacial layer of air, which significantly impairs the electrochemical properties, is not present. Compared to storage in ambient conditions, storage of CNSs in PBS did not significantly change their electrochemical characteristics over two weeks. We can infer one possible reason for this observation: if we assume that the concentration of structural defects decreases evenly over time in a liquid (as in ambient conditions), than the observed results imply that the decrease in electrochemical properties is somewhat counterbalanced and therefore not readily visible. If a small percentage of interfacial air became gradually replaced by water molecules, the effective surface area of the CNSs became more and more accessible over time, compensating for the aging of the CNSs. However, no firm conclusions can be drawn as the time of storage in PBS was much lower than it was for air.

4.4 CNS Biocompatibility

To our knowledge, no results on the biocompatibility of CNSs have been published to date. The biological experiments and findings described in this study are therefore an important next step into the assessment of the potential *in vitro* cytotoxicity of carbon nanomaterials. First, the growth of primary mouse hippocampal neurons on pristine, uncoated CNSs was severely impaired; cell viability was very poor and the few cells that could be observed were free-floating and clumped together. A relatively high proportion of these clumped cells were also dead or in necrosis or apoptosis. This low ability of neuronal cells to adhere and grow can partly be attributed to the high intrinsic hydrophobicity of pristine CNSs, for it is well known that cells need a hydrophilic surface for optimal adhesion and proliferation.[91] However, when CNS samples underwent a UV/O_3 treatment or were voltage-biased, cell viability was not significantly different, although the samples were now much more hydrophilic. Wettability of the CNS substrates is therefore not the only factor that plays a role in cell viability.

As most tissue cells are not adapted to living in suspension (unlike bacteria), they can only be cultured on a solid surface which, in this case, is provided by the CNSs. Even though the CNSs were made hydrophilic, cells vary in their requirements, and many do not adhere or grow unless the substrate is coated with, e.g., specific extracellular matrix components. Both pristine and surface-treated CNSs were therefore coated with PLL, a polymer that tends to attach to hydrophilic surfaces and enhances cell adhesion.[92-94] Although the coating of pristine CNSs with PLL initially seemed to increase cell viability, cell growth was strongly concentrated on the PDMS layer and not on the CNSs. This is a seemingly counterintuitive result, as both materials are highly hydrophobic and PLL generally attaches to hydrophilic surfaces. However, recent studies have shown that PLL can also adsorb onto nonpolar, hydrophobic PDMS surfaces from aqueous solution.[95-97] This adsorption is thought to occur through hydrophobic interactions between a hydrophobic component of the lysine units (the hydrocarbon chains, $\mathbf{C_4H_8}$-NH_3^+) and the surface.[95] To determine whether this hypothesis was also valid for the above-mentioned experiment, fluorescently labeled PLL was used to assess the relative binding affinity of PLL to PDMS and CNSs. It was, indeed, found that PLL shows a strong affinity for the PDMS but not for the CNSs, which consequently explains the strong observed affinity of the neuronal cells for the PDMS over the pristine CNSs when PLL is added.

When CNSs underwent a UV/O_3 treatment or were voltage-biased prior to PLL coating, cell viability increased dramatically. In both cases the cells preferably grew onto the CNSs, but a significant difference was found between the two treatments; while voltage-biased samples performed equally well as the PLL-coated glass coverslips (i.e. the reference), UV/O_3 treated CNSs coated with PLL yielded significantly lower results. A possible reason for the observed differences in viability might be the treatment itself; while UV/O_3 was found to be a good method to increase the electrochemical properties of the CNSs, their graphitic edges were also gradually being edged away. This stands in contrast to voltage-biasing, which had a less dramatic effect on the morphology and topography of the CNSs; even though they appeared more wrinkled, they maintained their sharp edges and flake-like structure. Voltage-biasing of CNSs might therefore preserve their high surface-area-

to-volume ratio better than a long UV/O_3 treatment, rendering more possible adsorption sites for the PLL molecules and more neuronal anchorage sites. More in-depth experiments are, however, required to support or refute this notion.

Carbon nanosheets have proven to be a suitable substrate for neuronal cell growth. Despite their high intrinsic hydrophobicity, CNSs can be made more hydrophilic with different techniques, such as UV/O_3 and voltage-biasing. This increase in hydrophilicity facilitates the adsorption of PLL, which has proven to be a necessary and very effective way to increase cellular adhesion and survival. It would be worthwhile to test other attachment factors in future experiments, such as laminin, fibronectin or collagen. Also other ways to oxidize the CNSs would be interesting to study. For example, chemical oxidation of CNTs with nitric acid or sulfuric acid can introduce oxygen-containing functionalities.[98-103] In addition, different plasma treatments, e.g. oxygen plasma, are expected to be good ways to functionalize the CNS surface.[104, 105]

Finally, while the biocompatibility of CNSs is demonstrated in this study, very little detail is known about the specific interactions of the neurons with the material, and how (or if) CNSs have an effect on cell physiology. The abundance of flake-like edges probably yields an excellent surface for cells to grasp onto, but the precise interaction mechanisms between neurons and CNSs is still unknown. For example, cells might simply grow on top of the CNSs, or the interaction can be more complicated, as in the case of CNS engulfment by the cellular membrane. Cryo-FIB/SEM investigation of this interaction can yield valuable and interesting new insights. Other questions that still need to be answered are: what is the effect of different CNS lengths on biocompatibility; are detached CNSs cytotoxic for cells; and what is the viability of other cell types? We hope that future research will address these gaps and will shed light on this emerging type of carbon nanomaterial.

5. Conclusion

In this study, the electrochemical properties and biocompatibility of CNSs have been investigated to determine whether this type of carbon nanomaterial is suited to be implemented in a high-throughput MEA setting. CNSs were hypothesized to be a promising new candidate to serve as neuro-electronic interconnects, with a unique interface (i.e. a high surface-area-to-volume ratio and abundance of knife-edge planes) that should make it possible to extracellularly measure the local variations of the electrical potential of electrogenic cells. Ideally, these signals are recorded with a high signal-to-noise ratio and a high spatiotemporal resolution; the latter meaning that the electrodes need to be scaled down to the size where they achieve single-cell addressability. Scaling down their dimensions, however, also yields a corresponding increase in impedance, and thus more noise. Besides of biocompatibility, highly wanted features of new electrode materials are therefore a low intrinsic impedance and a large CSC_c, i.e. a high recording and stimulation efficacy.

Initially, two different underlayer substrates were investigated, i.e. a 300 nm layer of aSi or TiN. While the CNSs grown on TiN demonstrated good adherence and robustness, the CNSs on the aSi substrates were very fragile and tended to detach from the surface very easily. Moreover, the strength of adhesion was also dependent from where the sample was acquired, i.e. the center or edge of the wafer. For both methane as acetylene-based CNSs, the wafers' edge yielded better results than the center, with the acetylene-based CNSs demonstrating the best electrochemical properties. More in-depth investigation revealed that CNSs, grown with a methane precursor gas, were thin and relatively unbranched. In contrast, acetylene yielded much thicker and more branched CNSs. Compared to the center, CNSs deposited on the wafers' edge were also longer, more branched and possessed a thinner base. All of these factors contribute to a higher effective surface area between the CNSs and electrolyte. However, static contact angle measurements revealed that both types of CNSs were very hydrophobic, with an average contact angle of 125°.

In order to increase their wettability and electrochemical properties, CNSs were exposed to a UV/O_3 treatment or voltage-biased. Generally, it was found that a UV/O_3 exposure time of 40-60 min was sufficient to increase the CSC_c with approximately 250% and to decrease the impedance by approximately 90%. The UV/O_3 treatment causes an abundance of oxygenated functional groups on the CNS surface, which lowered the contact angle to approximately 8°. This (super)hydrophilicity enhances the double-layer capacitance of the CNSs, as protons on the surrounding liquid can approach the CNS surface much more easily, which consequently results in a better electron transfer. However, prolonged UV/O_3 exposure also causes excessive etching damage to the CNSs, and the exposure time should be chosen in such a way that the CNSs are adequately covered with oxygenated functional groups, without simultaneously causing too much damage to their graphitic edges. The choice of the UV/O_3 exposure time primarily depends on the effective CNS surface area (i.e. length of the CNSs and degree of branching). Another efficient method to increase the electrochemical properties is by voltage-biasing the CNSs. The underlying mechanism is the irreversible electrochemical oxidation of the CNSs due to the presence of water electrolysis. When water decomposes into hydrogen and oxygen, both gases (but mainly hydrogen) are electrostatically adsorbed on the CNS surface.

Again, the adsorption of these gases increases the wettability, and thus the effective surface area between the CNSs and electrolyte. It was found that a 1.5 V bias (with a total charge density of 2.5 C cm^{-2} ph^{-1}) was able to generate higher CSC_c and lower impedance results compared to UV/O_3. Moreover, XSEM investigation showed no apparent damage to the CNSs; they appeared more wrinkled but maintained their sharp edges and flake-like structure.

Due to their high concentration of reactive graphitic edges, CNSs can be considered to be in a highly meta-stable state. After a storage period of two months in ambient air conditions, the electrochemical properties decreased in an exponential-like manner. We hypothesize that, during the aging process, the concentration of structural defects decreases and the CNSs gradually become more thermodynamically stable. After a certain amount of time, these properties will eventually stabilize and become fixed.

Finally, primary mouse hippocampal neurons were grown on CNS substrates to test biocompatibility and viability. It was found that pristine, uncoated CNSs did not support cell growth. Although their high intrinsic hydrophobicity is one rational reason, UV/O_3 treated and voltage-biased (i.e. hydrophilic) CNSs were also not able to promote the growth and survival of neurons. Only when hydrophilic CNSs were coated with PLL, cell viability was considerably higher. A significant difference, however, was found between PLL-coated samples that underwent a prior UV/O_3 treatment or were voltage-biased; the latter showing a higher cell viability then the former. We hypothesize that this difference is related to the treatment itself; while UV/O_3 gradually etches away the graphitic edges of the CNSs, voltage-biasing seemed to preserve their flake-like morphology better, rendering more possible adsorption sites for the PLL molecules and more neuronal anchorage sites.

Based on the experimental results and observations described above, CNSs have proven to be an attractive candidate for a new electrode material for bidirectional interfacing with electrogenic cells in a MEA setting. Important specific requirements, such as a low impedance, high CSC_c and biocompatibility, have all been met, and warrant the next step to patterned, micron-sized electrodes. Our findings demonstrate that CNS-based MEAs can have a major scientific and technological impact, and combined with CMOS IC technology, can yield tools for both *in vitro* and *in vivo* applications, including pharmacology, medical diagnostics, neuroscience and neuromedical research.

References

1. Braeken, D., et al., *Single-cell stimulation and electroporation using a novel 0.18 µm CMOS chip with subcellular-sized electrodes.* 32nd Annual International Conference of the IEEE EMBS, Buenos Aires, Argentinia, August 31 - September 4, 2010: p. 6473-6476.
2. Huys, R., et al., *Single-cell recording and stimulation with a 16k micro-nail electrode array integrated on a 0.18 [small mu]m CMOS chip.* Lab on a Chip, 2012. **12**(7): p. 1274-1280.
3. Huys, R., et al., *A novel 16k micro-nail CMOS-chip for in-vitro single-cell recording, stimulation and impedance measurements.* Engineering in Medicine and Biology Society (EMBC), Annual International Conference of the IEEE 2010: p. 2726 - 2729.
4. Neher, E. and B. Sakmann, *Single-channel currents recorded from membrane of denervated frog muscle fibres.* Nature, 1976. **260**(5554): p. 799-802.
5. Hamill, O.P., et al., *Improved patch-clamp techniques for high-resolution current recording from cells and cell-free membrane patches.* Pflügers Archiv European Journal of Physiology, 1981. **391**(2): p. 85-100.
6. Zhao, Y., et al., *Patch clamp technique: Review of the current state of the art and potential contributions from nanoengineering.* Proceedings of the Institution of Mechanical Engineers, Part N: Journal of Nanoengineering and Nanosystems, 2008. **222**(1): p. 1-11.
7. Comley, J., *Patchers versus Screeners - divergent opinion on high throughput electrophysiology.* Drug Discovery World, 2003. **4**: p. 47-57.
8. Hutzler, M., et al., *High-Resolution Multitransistor Array Recording of Electrical Field Potentials in Cultured Brain Slices.* J Neurophysiol, 2006. **96**(3): p. 1638-1645.
9. Eversmann, B., et al., *A 128 x 128 CMOS Biosensor Array for Extracellular Recording of Neural Activity.* Solid-State Circuits, 2003. **38**(12): p. 2306-2317.
10. Joye, N., A. Schmid, and Y. Leblebici, *Electrical modeling of the cell–electrode interface for recording neural activity from high-density microelectrode arrays.* Neurocomputing, 2009. **73**(1–3): p. 250-259.
11. Joye, N., A. Schmid, and Y. Leblebici. *A cell-electrode interface noise model for high-density microelectrode arrays*. in *Engineering in Medicine and Biology Society, 2009. EMBC 2009. Annual International Conference of the IEEE*. 2009.
12. Minnikanti, S. and N. Peixoto, *Implantable Electrodes with Carbon Nanotube Coatings*, in *Carbon Nanotubes Applications on Electron Devices*, J.M. Marulanda, Editor 2011, InTech. p. 556.
13. Cogan, S.F., *Neural Stimulation and Recording Electrodes.* Annual Review of Biomedical Engineering, 2008. **10**(1): p. 275-309.
14. Braeken, D., et al., *Localized electrical stimulation of in vitro neurons using an array of sub-cellular sized electrodes.* Biosensors and Bioelectronics, 2010. **26**(4): p. 1474-1477.
15. Heuschkel, M.O., et al., *A three-dimensional multi-electrode array for multi-site stimulation and recording in acute brain slices.* Journal of Neuroscience Methods, 2002. **114**(2): p. 135-148.
16. Heer, F., et al., *CMOS microelectrode array for bidirectional interaction with neuronal networks.* Solid-State Circuits, 2006. **41**(7): p. 1620 - 1629.
17. Pancrazio, J.J., et al., *Development and Application of Cell-Based Biosensors.* Annals of Biomedical Engineering, 1999. **27**(6): p. 697-711.
18. Berdondini, L., et al., *High-density electrode array for imaging in vitro electrophysiological activity.* Biosensors and Bioelectronics, 2005. **21**(1): p. 167-174.
19. Gross, G.W., et al., *The use of neuronal networks on multielectrode arrays as biosensors.* Biosensors and Bioelectronics, 1995. **10**(6-7): p. 553-567.
20. Huys, R., et al., *Novel concepts for improved communication between nerve cells and silicon electronic devices.* Solid-State Electronics, 2008. **52**(4): p. 533-539.
21. Hsu, H.-L., et al., *Flexible UV-Ozone-Modified Carbon Nanotube Electrodes for Neuronal Recording.* Advanced Materials, 2010. **22**(19): p. 2177-2181.
22. Yen, S.-J., et al., *The enhancement of neural growth by amino-functionalization on carbon nanotubes as a neural electrode.* Biosensors and Bioelectronics, 2011. **26**(10): p. 4124-4132.
23. Mazzatenta, A., et al., *Interfacing Neurons with Carbon Nanotubes: Electrical Signal Transfer and Synaptic Stimulation in Cultured Brain Circuits.* JNEUROSCI, 2007. **27**(26): p. 6931-6936.
24. Chen, Y.C., et al., *An active, flexible carbon nanotube microelectrode array for recording electrocorticograms.* Journal of Neural Engineering, 2011. **8**(3).
25. Minerbi, A., et al., *Long-Term Relationships between Synaptic Tenacity, Synaptic Remodeling, and Network Activity.* PLoS Biol, 2009. **7**(6): p. e1000136.

26. Bean, B.P., *The action potential in mammalian central neurons.* Nat Rev Neurosci, 2007. **8**(6): p. 451-465.
27. Hodgkin, A.L. and R.D. Keynes, *Active transport of cations in giant axons from Sepia and Loligo.* The Journal of Physiology, 1955. **128**(1): p. 28-60.
28. Jens Chr, S., *The influence of some cations on an adenosine triphosphatase from peripheral nerves.* Biochimica et Biophysica Acta, 1957. **23**(0): p. 394-401.
29. Alberts, B., et al., *Molecular Biology of the Cell*. 4 ed2002: Garland Science. 1616.
30. Hierlemann, A., et al., *Growing Cells Atop Microelectronic Chips: Interfacing Electrogenic Cells In Vitro With CMOS-Based Microelectrode Arrays.* Proceedings of the IEEE 2011. **99**(2): p. 252 - 284.
31. Levin, K.H. and H.O. Luders, *Comprehensive Clinical Neurophysiology*. 1 ed2000: Saunders. 627.
32. Bear, M.F., B.W. Connors, and M.A. Paradiso, *Properties of the action potential*, in *Neuroscience: exploring the brain*2007, Lippincott Williams & Wilkins. p. 76-80.
33. Bear, M.F., B.W. Connors, and M.A. Paradiso, *The ionic basis of the resting membrane potential*, in *Neuroscience: exploring the brain*2007, Lippincott Williams & Wilkins. p. 61-71.
34. Cofer, D. *Neuron Basics*. 2002; Available from: http://www.mindcreators.com/NeuronBasics.htm.
35. Graham, A.H.D., et al., *Commercialisation of CMOS Integrated Circuit Technology in Multi-Electrode Arrays for Neuroscience and Cell-Based Biosensors.* Sensors, 2011. **11**(5): p. 4943-4971.
36. Chang, J.-h., et al., *Fitting Improvement Using a New Electrical Circuit Model for the Electrode-Electrolyte Interface.* Proceedings of the 3rd International IEEE EMBS Conference on Neural Engineering, 2007: p. 572-574.
37. Franks, W., et al., *Impedance characterization and modeling of electrodes for biomedical applications.* IEEE Transactions on Biomedical Engineering, 2005. **52**(2): p. 1295-1302.
38. Jorcin, J.-B., et al., *CPE analysis by local electrochemical impedance spectroscopy.* Electrochimica Acta, 2006. **51**(8–9): p. 1473-1479.
39. Wei, X.F. and W.M. Grill, *Impedance characteristics of deep brain stimulation electrodes in vitro and in vivo.* Journal of Neural Engineering, 2009. **6**(4): p. 046008.
40. Kim, J., *Development of thin film polymer flexible microelectrode arrays for neural interface applications*, 2008, The University of Wisconsin - Madison. p. 140.
41. Żółtowski, P., *On the electrical capacitance of interfaces revealing constant phase element behaviour.* J. Electroanal. Chem, 1998. **443**: p. 149-154.
42. Macdonald, J.R., *Impedance Spectroscopy: Emphasizing Solid Materials and Analysis*1987, New York: John Wiley & Sons.
43. Novoselov, K.S., et al., *Two-dimensional atomic crystals.* Proc Natl Acad Sci U S A, 2005. **102**(30): p. 10451–10453.
44. Chen, T., et al., *High throughput exfoliation of graphene oxide from expanded graphite with assistance of strong oxidant in modified Hummers method.* J. Phys.: Conf. Ser., 2009. **188**(1): p. 012051.
45. Sutter, P., *Epitaxial graphene: How silicon leaves the scene.* Nat Mater, 2009. **8**(3): p. 171-172.
46. Berger, C., et al., *Ultrathin epitaxial graphite: 2D electron gas properties and a route toward graphene-based nanoelectronics.* J. Phys. Chem., 2004. **108**(52): p. 19912-16.
47. Emtsev, K.V., et al., *Interaction, growth, and ordering of epitaxial graphene on SiC{0001} surfaces: A comparative photoelectron spectroscopy study.* Physical Review B, 2008. **77**(15): p. 155303.
48. Malesevic, A., et al., *Synthesis of few-layer graphene via microwave plasma-enhanced chemical vapour deposition.* Nanotechnology, 2008. **19**(30): p. 305604.
49. Shang, N.G., et al., *Catalyst-Free Efficient Growth, Orientation and Biosensing Properties of Multilayer Graphene Nanoflake Films with Sharp Edge Planes.* Adv. Funct. Mat., 2010. **18**(21): p. 3506-3514.
50. Soin, N., et al., *Microstructural and electrochemical properties of vertically aligned few layered graphene (FLG) nanoflakes and their application in methanol oxidation.* Materials Chemistry and Physics, 2011. **129**(3): p. 1051-1057.
51. Wang, Z., M. Shoji, and H. Ogata, *Carbon nanosheets by microwave plasma enhanced chemical vapor deposition in CH_4-Ar system.* Applied Surface Science, 2011. **257**(21): p. 9082-9085.
52. Zhang, J., et al., *Low substrate temperature synthesis of carbon nanowalls by ultrasonic spray pyrolysis.* Thin Solid Films, 2011. **519**(13): p. 4162-4165.
53. Mazzatenta, A., et al., *Interfacing neurons with carbon nanotubes: Electrical signal transfer and synaptic stimulation in cultured brain circuits.* Journal of Neuroscience, 2007. **27**(26): p. 6931-6936.
54. Ben-Jacob, E. and Y. Hanein, *Carbon nanotube micro-electrodes for neuronal interfacing.* Journal of Materials Chemistry, 2008. **18**(43): p. 5181-5186.

55. Gabay, T., et al., *Electro-chemical properties of carbon nanotube based multi-electrode arrays.* Nanotechnology, 2007. **18**: p. 035201
56. Smart, S.K., et al., *The biocompatibility of carbon nanotubes.* Carbon, 2006. **44**(6): p. 1034-1047.
57. Hafner, J.H., et al., *Catalytic growth of single-wall carbon nanotubes from metal particles.* Chemical Physics Letters, 1998. **296**(1-2): p. 195-202.
58. Pumera, M., *Carbon Nanotubes Contain Residual Metal Catalyst Nanoparticles even after Washing with Nitric Acid at Elevated Temperature Because These Metal Nanoparticles Are Sheathed by Several Graphene Sheets.* Langmuir, 2007. **23**(11): p. 6453-6458.
59. Guo, L., et al., *Iron Bioavailability and Redox Activity in Diverse Carbon Nanotube Samples.* Chemistry of Materials, 2007. **19**(14): p. 3472-3478.
60. Liu, H., et al., *Self-Assembly of Large-Scale Micropatterns on Aligned Carbon Nanotube Films.* Angewandte Chemie International Edition, 2004. **43**(9): p. 1146-1149.
61. Correa-Duarte, M.A., et al., *Fabrication and Biocompatibility of Carbon Nanotube-Based 3D Networks as Scaffolds for Cell Seeding and Growth.* Nano Letters, 2004. **4**(11): p. 2233-2236.
62. De Volder, M., et al., *Diverse 3D Microarchitectures Made by Capillary Forming of Carbon Nanotubes.* Advanced Materials, 2010. **22**(39): p. 4384-4389.
63. Vansweevelt, R., et al., *Biological modification of carbon nanowalls with DNA strands and hybridization experiments with complementary and mismatched DNA.* Chem. Phys. Lett., 2010. **485**(1-3): p. 196-201.
64. Hu, H., et al., *Chemically Functionalized Carbon Nanotubes as Substrates for Neuronal Growth.* Nano Letters, 2004. **4**(3): p. 507-511.
65. Watts, K.C. and O. Husain, *Optimal use of the cationic polyelectrolyte poly-L-lysine in the preparation of cell monolayers for diagnostic cytopathology.* Journal of clinical pathology, 1984. **37**(7): p. 829-31.
66. Kikkawa, Y., et al., *Integrin binding specificity of laminin-10/11: laminin-10/11 are recognized by alpha 3 beta 1, alpha 6 beta 1 and alpha 6 beta 4 integrins.* Journal of Cell Science, 2000. **113**(5): p. 869-876.
67. Nishiuchi, R., et al., *Ligand-binding specificities of laminin-binding integrins: A comprehensive survey of laminin–integrin interactions using recombinant α3β1, α6β1, α7β1 and α6β4 integrins.* Matrix Biology, 2006. **25**(3): p. 189-197.
68. Huang, Y.-C., et al., *Effects of laminin-coated carbon nanotube/chitosan fibers on guided neurite growth.* Journal of Biomedical Materials Research Part A, 2011. **99A**(1): p. 86-93.
69. Hamburg, U. *Carbon Nanowalls*. November 29, 2011; Available from: http://www.chemie.uni-hamburg.de/pc/mews/research/nanotubes_e.html.
70. Brewer, G.J., *Serum-free B27/neurobasal medium supports differentiated growth of neurons from the striatum, substantia nigra, septum, cerebral cortex, cerebellum, and dentate gyrus.* Journal of Neuroscience Research, 1995. **42**(5): p. 674-683.
71. Wang, Z., et al., *Polarity-Dependent Electrochemically Controlled Transport of Water through Carbon Nanotube Membranes.* Nano Letters, 2007. **7**(3): p. 697-702.
72. Zhu, L., et al., *Electrowetting of Aligned Carbon Nanotube Films.* The Journal of Physical Chemistry B, 2006. **110**(32): p. 15945-15950.
73. *Using Phosphate-Buffered Saline (PBS) in Biochemical and Cell Biology Research*. Available from: http://biologicalworld.com/pbs.htm.
74. Biocompare. *Calcein AM – For Live Cell Staining*. 06/08/2009; Available from: http://www.biocompare.com/Application-Notes/42607-Calcein-AM-For-Live-Cell-Staining/.
75. Invitrogen. *Propidium Iodide Nucleic Acid Stain*. 2006; Available from: http://probes.invitrogen.com/media/pis/mp01304.pdf.
76. McKeehan, W.L., *Methods for Preparation of Media, Supplements, and Substrata for Serum-free Animal Cell Culture*1984, NY: A.R. Liss.
77. Wu, Y., et al., *Carbon nanowalls and related materials.* Journal of Materials Chemistry, 2004. **14**(4): p. 469-477.
78. Chuang, A.T.H., et al., *Three-dimensional carbon nanowall structures.* Applied Physics Letters, 2007. **90**(12): p. 123107-123107-3.
79. Aria, A.I. and M. Gharib, *Reversible Tuning of the Wettability of Carbon Nanotube Arrays: The Effect of Ultraviolet/Ozone and Vacuum Pyrolysis Treatments.* Langmuir, 2011. **27**(14): p. 9005-9011.
80. Kim, Y.-T., et al., *Drastic change of electric double layer capacitance by surface functionalization of carbon nanotubes.* Applied Physics Letters, 2005. **87**(23): p. 234106.
81. Senftle, F.E., J.R. Grant, and F.P. Senftle, *Low-voltage DC/AC electrolysis of water using porous graphite electrodes.* Electrochimica Acta, 2010. **55**(18): p. 5148-5153.

82. Allouche, A., et al., *Hydrogen adsorption on graphite (0001) surface: A combined spectroscopy--density-functional-theory study.* The Journal of Chemical Physics, 2005. **123**(12): p. 124701.
83. Züttel, A., et al., *Model for the hydrogen adsorption on carbon nanostructures.* Applied Physics A: Materials Science & Processing, 2004. **78**(7): p. 941-946.
84. Chambers, A., et al., *Hydrogen Storage in Graphite Nanofibers.* The Journal of Physical Chemistry B, 1998. **102**(22): p. 4253-4256.
85. Giraudet, S. and Z. Zhu, *Electrochemical Hydrogen Adsorption Onto Graphene Nanosheets.* Journal of Nano Energy and Power Research, 2011. **1**(1): p. 82-84.
86. Qu, D., *Mechanism for electrochemical hydrogen insertion in carbonaceous materials.* Journal of Power Sources, 2008. **179**(1): p. 310-316.
87. Sorescu, D.C., K.D. Jordan, and P. Avouris, *Theoretical Study of Oxygen Adsorption on Graphite and the (8,0) Single-walled Carbon Nanotube.* The Journal of Physical Chemistry B, 2001. **105**(45): p. 11227-11232.
88. Giannozzi, P., R. Car, and G. Scoles, *Oxygen adsorption on graphite and nanotubes.* The Journal of Chemical Physics, 2003. **118**(3): p. 1003-1006.
89. Yang, L., et al., *Aging of nanocarbons in ambient conditions: Probable metastability of carbon nanotubes.* Journal of Colloid and Interface Science, 2009. **338**(1): p. 128-134.
90. Kim, S., et al., *Room-temperature metastability of multilayer graphene oxide films.* Nat Mater, 2012. **11**(6): p. 544-549.
91. Thull, R., *Tissue-implant interaction*, in *Metals as biomaterials*, H.J.B. J.A. Helsen, Editor 1998, John Wiley & Sons: New York. p. 291-315.
92. Choi, J.S., et al., *Synthesis of a Barbell-like Triblock Copolymer, Poly(l-lysine) Dendrimer-block-Poly(ethylene glycol)-block-Poly(l-lysine) Dendrimer, and Its Self-Assembly with Plasmid DNA.* Journal of the American Chemical Society, 2000. **122**(3): p. 474-480.
93. Kenausis, G.L., et al., *Poly(l-lysine)-g-Poly(ethylene glycol) Layers on Metal Oxide Surfaces: Attachment Mechanism and Effects of Polymer Architecture on Resistance to Protein Adsorption†.* The Journal of Physical Chemistry B, 2000. **104**(14): p. 3298-3309.
94. Toncheva, V., et al., *Novel vectors for gene delivery formed by self-assembly of DNA with poly(l-lysine) grafted with hydrophilic polymers.* Biochimica et Biophysica Acta (BBA) - General Subjects, 1998. **1380**(3): p. 354-368.
95. Lee, S. and N.D. Spencer, *Poly(l-lysine)-graft-poly(ethylene glycol): a versatile aqueous lubricant additive for tribosystems involving thermoplastics.* Lubrication Science, 2008. **20**(1): p. 21-34.
96. Lee, S. and J. Vörös, *An Aqueous-Based Surface Modification of Poly(dimethylsiloxane) with Poly(ethylene glycol) to Prevent Biofouling.* Langmuir, 2005. **21**(25): p. 11957-11962.
97. Lee, S. and N.D. Spencer, *Adsorption Properties of Poly(l-lysine)-graft-poly(ethylene glycol) (PLL-g-PEG) at a Hydrophobic Interface: Influence of Tribological Stress, pH, Salt Concentration, and Polymer Molecular Weight.* Langmuir, 2008. **24**(17): p. 9479-9488.
98. Zhang, J., et al., *Effect of Chemical Oxidation on the Structure of Single-Walled Carbon Nanotubes.* The Journal of Physical Chemistry B, 2003. **107**(16): p. 3712-3718.
99. Kim, B. and W.M. Sigmund, *Functionalized Multiwall Carbon Nanotube/Gold Nanoparticle Composites.* Langmuir, 2004. **20**(19): p. 8239-8242.
100. Sumanasekera, G.U., et al., *Electrochemical Oxidation of Single Wall Carbon Nanotube Bundles in Sulfuric Acid.* The Journal of Physical Chemistry B, 1999. **103**(21): p. 4292-4297.
101. Naseh, M.V., et al., *Functionalization of Carbon Nanotubes Using Nitric Acid Oxidation and DBD Plasma.* World Academy of Science, Engineering and Technology, 2009. **49**: p. 177-179.
102. Tchoul, M.N., et al., *Effect of Mild Nitric Acid Oxidation on Dispersability, Size, and Structure of Single-Walled Carbon Nanotubes.* Chemistry of Materials, 2007. **19**(23): p. 5765-5772.
103. Rosca, I.D., et al., *Oxidation of multiwalled carbon nanotubes by nitric acid.* Carbon, 2005. **43**(15): p. 3124-3131.
104. Chirila, V., G. Marginean, and W. Brandl, *Effect of the oxygen plasma treatment parameters on the carbon nanotubes surface properties.* Surface and Coatings Technology, 2005. **200**(1–4): p. 548-551.
105. Kalbacova, M., et al., *Controlled oxygen plasma treatment of single-walled carbon nanotube films improves osteoblastic cells attachment and enhances their proliferation.* Carbon, 2011. **49**(9): p. 2926-2934.

Supplemental Information

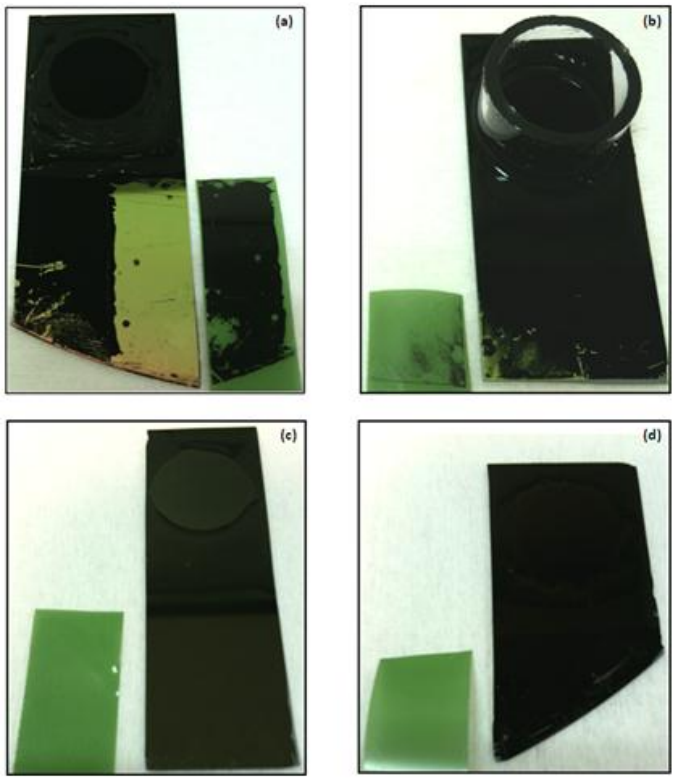

Fig. S1. Scotch tape adhesion test of CNSs deposited on aSi (a,b) and TiN (c,d) wafer substrates. (a) CNSs grown on the edge of aSi substrates completely detached from the surface, while (b) CNSs deposited on the center demonstrated better adhesion, with only a small percentage of sheets that was transferred to the tape (attached ring of no relevance). (c,d) Adhesion tests on both the center and edge of TiN substrates were not able to detach any deposited CNSs from the surface.

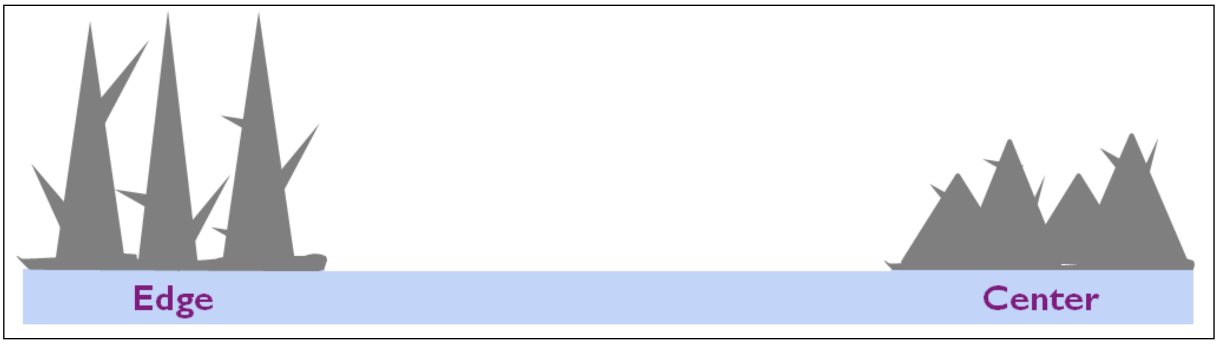

Fig. S2. Schematic illustration showing the difference in CNS structure between the edge and center of the wafer. Sheets ŘŜǇŽăʎǗŜŘ ŽɣƴǗKŜ ǿI·ŦŜŊăΩ ŜŘƎŜ I·ŊŜ ƭŽɣƎŜŊΣ I·ŊŜ ʏŽŊŜ ōŊI·ɣǑKŜŘ I·ɣŘ ǇŽăăŜăă I· ǗKʎɣǗŜŊ ōI·ăŜΣ ǿKʎƭŜ ǑŜɣǗŜŊ /b{ă I·ŊŜ ăKŽŊǗŜŊ and have a much broader base.

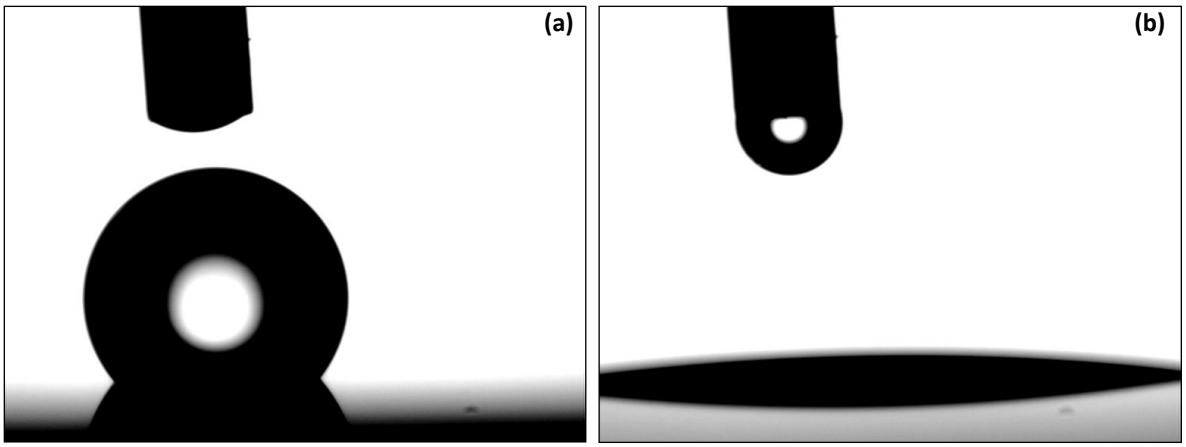

Fig. S3. Contact angle measurements (a) before and (b) after 10 min of UV/O_3. Measured contact angles were approximately 125° and 8° respectively.

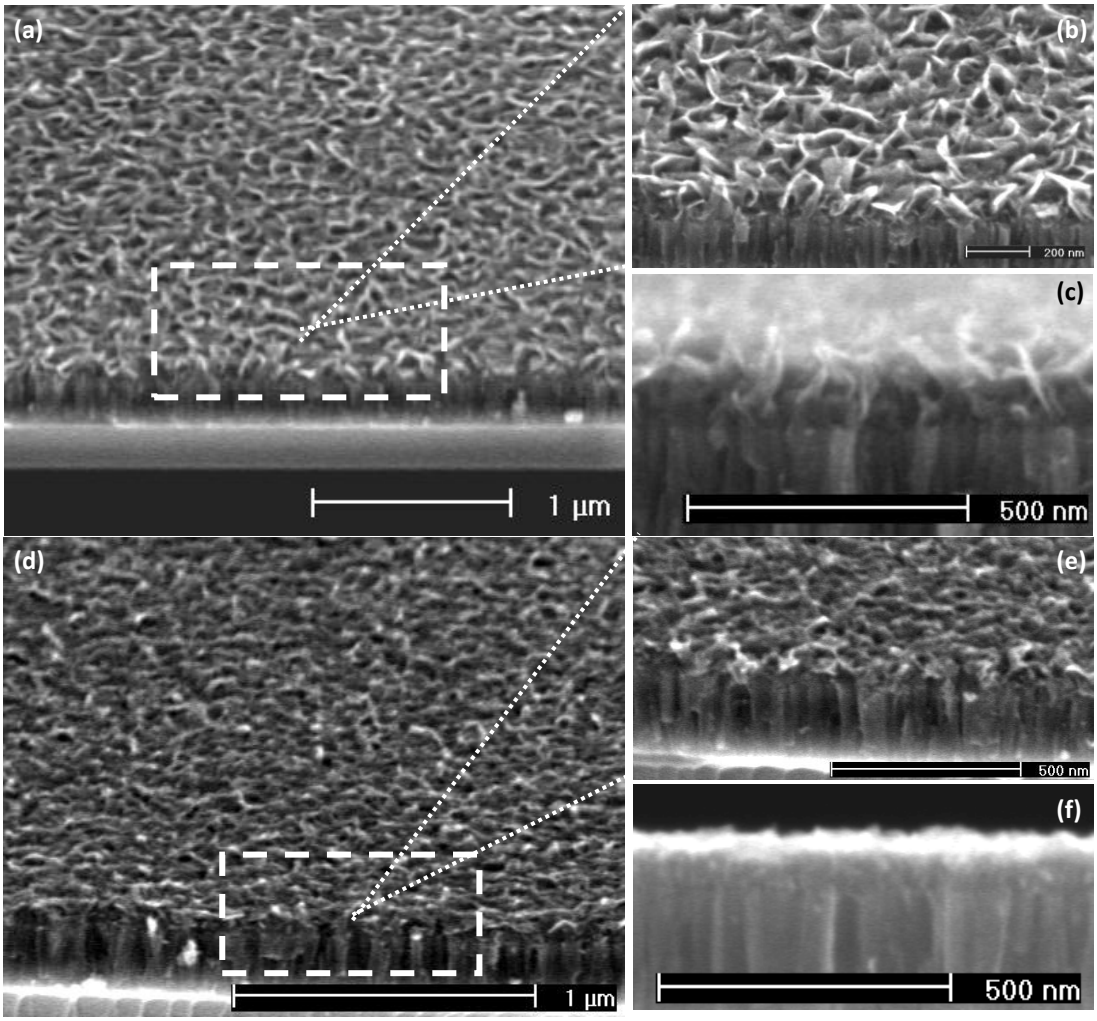

Fig. S4. XSEM photographs of UV/O_3 treated CNSs. (a) CNSs exposed to 40 min of UV/O_3 kept their knife-like structure with plenty of graphitic edges. The area in the white dashed box is magnified in (b). (c) Cross-sectional view of the CNSs attached to the TiN substrate. (d) UV/O_3 treated CNSs for a total of 80 min. The CNSs are almost completely etched away. The area in the white dashed box is magnified in (e). (f) Cross-sectional view; the sharp edges disappeared, leaving only a thin layer of carbon behind.

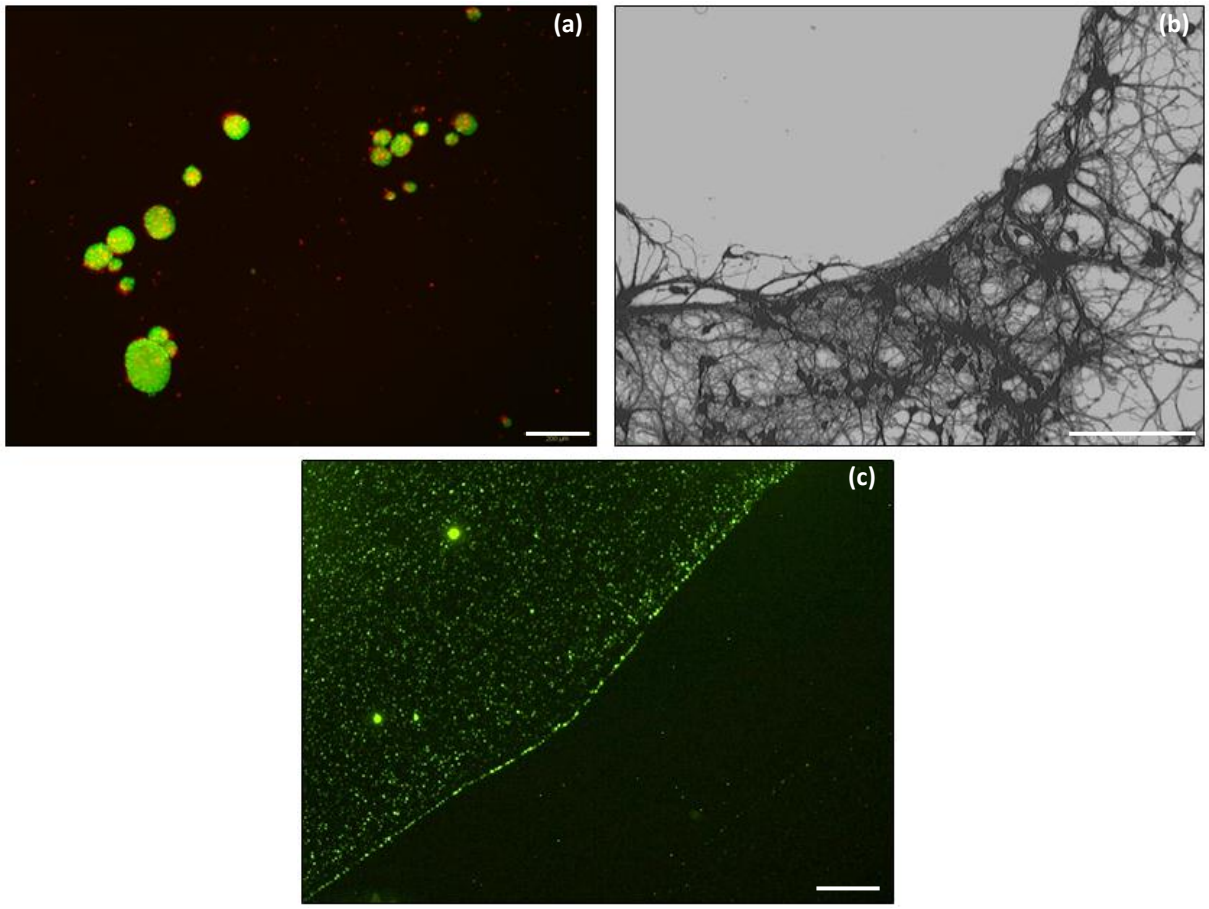

Fig. S5. (a) Free-floating clumps of cells. The scale bar corresponds to 200 µm. (b) Digitally enhanced image of neurons and their projections. After coating with PLL, neuronal growth was strongly concentrated on the PDMS layer, but not on the pristine CNSs. The scale bar corresponds to 100 µm (c) Coating with fluorescently labeled PLL revealed that PLL had a strong affinity for the PDMS, but not for the pristine CNSs. The scale bar corresponds to 200 µm.

Auteursrechtelijke overeenkomst

Ik/wij verlenen het wereldwijde auteursrecht voor de ingediende eindverhandeling:
Characterization of carbon nanosheets as an electrode material and biological interface for advanced microelectrode arrays

Richting: **master in de biomedische wetenschappen-bio-elektronica en nanotechnologie**
Jaar: **2012**

in alle mogelijke mediaformaten, - bestaande en in de toekomst te ontwikkelen - , aan de Universiteit Hasselt.

Niet tegenstaand deze toekenning van het auteursrecht aan de Universiteit Hasselt behoud ik als auteur het recht om de eindverhandeling, - in zijn geheel of gedeeltelijk -, vrij te reproduceren, (her)publiceren of distribueren zonder de toelating te moeten verkrijgen van de Universiteit Hasselt.

Ik bevestig dat de eindverhandeling mijn origineel werk is, en dat ik het recht heb om de rechten te verlenen die in deze overeenkomst worden beschreven. Ik verklaar tevens dat de eindverhandeling, naar mijn weten, het auteursrecht van anderen niet overtreedt.

Ik verklaar tevens dat ik voor het materiaal in de eindverhandeling dat beschermd wordt door het auteursrecht, de nodige toelatingen heb verkregen zodat ik deze ook aan de Universiteit Hasselt kan overdragen en dat dit duidelijk in de tekst en inhoud van de eindverhandeling werd genotificeerd.

Universiteit Hasselt zal mij als auteur(s) van de eindverhandeling identificeren en zal geen wijzigingen aanbrengen aan de eindverhandeling, uitgezonderd deze toegelaten door deze overeenkomst.

Voor akkoord,

Cools, Jordi

Datum: **11/06/2012**